



Citation for published version:

Fan, W, Dai, Z, Zhang, B, He, L, Pan, M, Yi, J & Liu, T 2024, 'HyExo: A Novel Quasi-Passive Hydraulic Exoskeleton for Load-Carrying Augmentation', *IEEE - ASME Transactions on Mechatronics*.
<https://doi.org/10.1109/TMECH.2024.3391350>

DOI:

[10.1109/TMECH.2024.3391350](https://doi.org/10.1109/TMECH.2024.3391350)

Publication date:

2024

Document Version

Peer reviewed version

[Link to publication](#)

Publisher Rights

CC BY

University of Bath

Alternative formats

If you require this document in an alternative format, please contact:
openaccess@bath.ac.uk

General rights

Copyright and moral rights for the publications made accessible in the public portal are retained by the authors and/or other copyright owners and it is a condition of accessing publications that users recognise and abide by the legal requirements associated with these rights.

Take down policy

If you believe that this document breaches copyright please contact us providing details, and we will remove access to the work immediately and investigate your claim.

HyExo: A Novel Quasi-Passive Hydraulic Exoskeleton for Load-Carrying Augmentation

Journal:	<i>Transactions on Mechatronics</i>
Manuscript ID	TMECH-09-2023-16404.R1
Manuscript Type:	Regular paper
Date Submitted by the Author:	13-Dec-2023
Complete List of Authors:	Fan, Wu; Dai, Zhe Zhang, Bin; China Jiliang University College of Mechanical and Electrical Engineering He, Long Pan, Min Yi, Jingang (AIM TE); Rutgers, The State University of New Jersey, Mechanical and Aerospace Engineering Liu, Tao; Zhejiang University, School of Mechanical Engineering
Keywords:	Pneumatics & hydraulics < Actuators and sensors, Energy harvesting < System integration, Human-robot interaction, haptics & teleoperation < Robotics
Are any of authors IEEE Member?:	Yes
Are any of authors ASME Member?:	Yes
Note: The following files were submitted by the author for peer review, but cannot be converted to PDF. You must view these files (e.g. movies) online.	
HyExo3.mp4	

HyExo: A Novel Quasi-Passive Hydraulic Exoskeleton for Load-Carrying Augmentation

Wu Fan, Zhe Dai, Bin Zhang, Long He, Min Pan, and Jingang Yi, Tao Liu

Abstract—The development of assistive lower-limb exoskeletons gains prominence for human load-carrying augmentation. Hydraulic transmission has attractive hydrostatic features and lower inertia at the end of human limbs. However, few hydraulic lower-limb exoskeletons were developed with low energy consumption and light weight. In this article, we introduce HyExo, a quasi-passive hydraulic exoskeleton that is built on a lightweight rotary cage valve (RCV) block with a fast response and low energy consumption of 1.55 W. Based on the RCV block, we propose an optimization-based regulator for joint energy distribution to harvest and release the hydraulic energy among joints during the stance phase. The interaction force model and control of the novel non-anthropomorphic structure are presented and evaluated. The load-supporting effect was investigated and validated through human subject experiments. The results show that with an assisting fluid pressure of 2.5 MPa, HyExo can transfer a mean force of 237 N to the ground. Meanwhile, the impact of wearing HyExo on gait is analyzed. The metabolic expenditure test shows that HyExo can slow the increasing rate in metabolic cost as load increases. Compared to a regular backpack, walking with HyExo to carry 30kg of weight reduces wears' metabolic energy expenditure by 7.8%.

Index Terms—Human augmentation, hydraulic/pneumatic actuators, prosthetics, exoskeletons, energy harvesting

I. INTRODUCTION

It is common for human walkers to carry and transport heavy loads on level or sloped ground, or even on unpaved, complex terrains. To improve transport efficiency and reduce possible musculoskeletal disorders due to heavy load, many exoskeleton research work focus on augmenting the human load-carrying capability. The design of load-carrying exoskeletons requires two main features: transmitting the payload force to the ground and reducing the energy consumption for both the human walker and wearable assistive devices. Traditional hydraulic exoskeletons have fully actuated joints, and the control strategy of servo valves relies on precise gait analysis and tracking (e.g., [1]). In general, valve-controlled

hydraulic exoskeletons provide excessive energy that is wasted due to the valve throttling and overflow [2]. For instance, the BLEEX consumes approximately 2.27 kW of hydraulic power, 220 W of electronic devices, and the entire robotic system weighs more than 40 kg [3]. Such fully powered exoskeletons are energy-inefficient and heavy due to the high-power prime mover and batteries.

Taking advantage of the high power density and transparency of hydraulic transmission, passive damping control has been applied to prostheses and exoskeletons. EXO presented in [4] and Exobuddy in [5] applied variable dampers to share supporting force during the human walking stance phase. Quasi-active joints were proposed by actuating the damper valve or controlling the viscosity of magnetorheological fluid with high power density and light weight. However, energy is dissipated at the orifice of damper valves, and such actuators' function is limited because they cannot do positive work. Some research works tried to regulate energy among joints by mechanical structures (e.g., [6], [7]), or energy cycling in a single joint, to help propulsion at different stages [8]. An adaptive energy regulation is required to determine when and where the energy should be harvested or released.

By far, most lower-limb exoskeletons were designed anthropomorphically. To accurately track the wearer's motion and reduce the misalignment between the exoskeleton and the human wearer, many efforts were made for accurately predicting walking dynamics and intention [9]. Adaptive robust control and self-adapting compliant joint were designed to address the nonlinearity and uncertainties of the hydraulic system or reduce the misalignment between the exoskeleton and the wearer [10], [11]. To bypass these problems, some non-anthropomorphic designs were proposed and tested, especially supernumerary limbs. Khazoom *et al.* [12] proposed a supernumerary leg powered by magnetorheological actuators to assist human locomotion. Similarly, extra robotic legs were designed to assist load-carrying [13]. Non-anthropomorphic structures, by contrast, have less physical connection with the human body and can provide more direct force transmission.

With external energy input, powered exoskeletons reduce the metabolic energy expenditure of ambulation [14]. Theoretically, transporting load horizontally at an even speed with no height variation consumes no energy. Therefore, it is desirable to develop a device to provide support force for the load along with the wearer's gait without consuming extra energy on level ground. In our previous work [15], a hydrostatic actuator was tested on a robotic leg to demonstrate high load-carrying capacity. In this paper, we propose a novel quasi-passive hydrostatic exoskeleton, called HyExo, which

This work was supported in part by the NSFC Grant No. 52175033 and No. U21A20120; the Zhejiang Provincial Natural Science Foundation of China under Grant No. LZ20E050002. (Corresponding author: Tao Liu.)

W. Fan, T. Liu, and Z. Dai are with the State Key Laboratory of Fluid Power & Mechatronic Systems, School of Mechanical Engineering, Zhejiang University, 310027, Hangzhou, China (e-mail: zjufanwu@zju.edu.cn; daizhe@zju.edu.cn; liutao@zju.edu.cn).

B. Zhang is with the College of Mechanical and Electrical Engineering, China Jiliang University, Hangzhou 310018, zhangbin@cjlu.edu.cn

L. He is with the Zhiyuan Research Institute, 310024, Hangzhou, China (e-mail: helong@zy-cs.com.cn).

M. Pan is with the Department of Mechanical Engineering at the University of Bath, BA2 7AY Bath, UK (e-mail:mp351@bath.ac.uk).

J. Yi is with the Department of Mechanical and Aerospace Engineering, Rutgers University, Piscataway, NJ 08854 USA (e-mail:jgyi@rutgers.edu).

modulates the energy between different joints and assists in carrying heavy loads. HyExo has two 7 degrees-of-freedom (DOFs) in each non-anthropomorphic leg that connects the wearer's back and toe. The main feature of the HyExo lies in a new lightweight rotary cage valve (RCV) with low power (around 0.8 W) and fast response (within 50 ms). Benefiting from the attractive feature of the RCV, HyExo does not need heavy power source and prime mover. A real-time optimization scheme is proposed to determine the switching time of RCV blocks for maximizing the supporting impulse and adaptively coordinating with human walking gaits.

Multiple experiments involving different subjects were conducted to evaluate the performance of HyExo, which included load-sharing tests on terrains with degrees of incline, gait analysis at multiple speeds, and energy expenditure tests. The main contributions of the work is twofold. First, the proposed RCV is a novel, lightweight, and energy-efficient hydraulic mechatronic component that control the energy flow among exoskeleton joints. Secondly, HyExo is a non-tethered, non-anthropomorphic exoskeleton that provides large load-carrying force for general human walking gaits.

The remainder of the paper is organized as follows. Section II presents the design of HyExo and RCV. The HyExo control is discussed in Section III. We present the experiments and human subject results in Section IV. Finally, concluding summary is discussed in Section VI.

II. HYEXO DESIGN AND MECHANISM

A. Mechanical Design of HyExo

Fig. 1 shows HyExo's main mechanical design and components. The non-anthropomorphic leg rods provide force transmission from the toe point (TP), through the knee point (KP), to the back point (BP). BPs are as medialized as possible to reduce the unbalanced coronal torque generated by the support force, preventing severe rolling sloshing of the backpack during walking. Instead of at the heel, the force bearing point on foot is set at the toe. According to [16], as the payload increases, the greatest location with positive

work was attributable to the ankle during push-off (45-60% of stride time). If the payload force is transmitted to the TP, the ankle joint would be relaxed from the load of pushing the leg upward during the pre-swing stage of a gait cycle [17]. As illustrated in Fig. 1(a), the TP, KP, and BP are designed in a plane perpendicular to the axis of the knee joint, and this feature avoids generating a bending moment at the knee joint and therefore reduces the potential risk of abrasion. The elastic elements are set to balance the weight of legs and the backpressure.

Fig. 1(b) shows HyExo's main components, including the embedded systems and actuators. As listed in Fig. 1(c), the entire HyExo weighs 13.87 kg, including a 2000 mAh 16 V LiPo battery and a 10000 mAh 5 V LiPo battery. The rods and joint connections are made of aluminum alloy. The cylinder barrel is aluminum lined and reinforced by carbon fiber composite [18]. The RCV block weighs only 1.2 kg and manages the connections between cylinders and vessels. To measure the joint angle at KPs, BPs, and the toe flip angle, six 12-bit magnetic encoders are installed. At top of the stirrup, a load cell is used to record the interaction force in the instep direction, and a spherical hinge to act as a 3-DOF joint. The BP joint has 2 DOFs, and the knee joint is 1-DOF. One more DoF is remained for toe extension at the stirrup. As shown in Fig. 1(a), there are 7 DOFs for each leg of HyExo to fulfill any position and orientation of the foot toward the back. See Fig. 1(b), at the bottom of a stirrup, two laminated force sensors made of force sensitive resistor (FSR) detect whether the heels and toes are contacting the ground.

B. Hydraulic Circuit and RCV Block

Fig. 2 (a) illustrates the schematic of the hydraulic circuits of HyExo. Without a pump circulating the fluid, all the pipes have bilateral flow and are divided into the high- and low-pressure sides. The exoskeleton is non-tethered and portable vessels are built-in to provide fluid and maintain the pressure. The low-pressure side is connected to the pressurized tank with a pressure of 2 to 3 bar, and the high-pressure side is connected

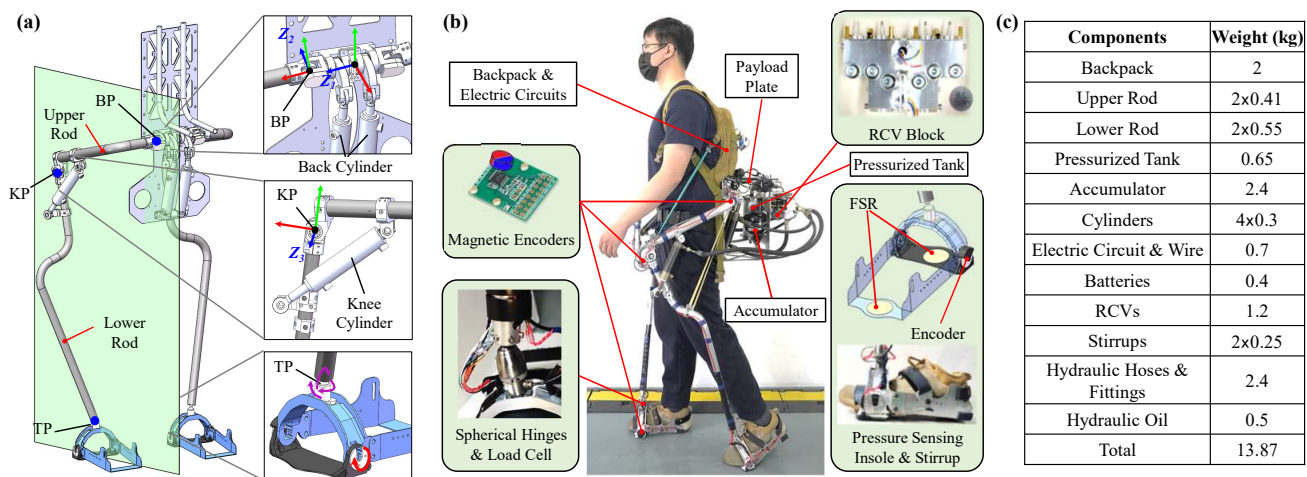


Fig. 1. (a) HyExo's non-anthropomorphic architecture and DOFs. The blue arrows represent the axis of motion joints, and the violet curved arrows indicate three rotary DoFs at TP. The green transparent plane indicates that the TP, KP, and BP are in a plane perpendicular to the knee joint axis (Z_3). (b) The main components and several close-up shots of key parts. (c) A list of component weights.

to an accumulator with a pre-charged pressure of 1 MPa. In design, cylinders act multi-functionally as both an actuator and a pump to provide the high-pressure oil to the accumulator under the RCVs' control. During the wearer's stance phase on level ground, the knee cylinder is compressed and harvests energy. At the same time, the back cylinder extends to assist the wearer's motion and release energy. During the swing phase, all the cylinder chambers are connected to the low-pressure side without assistance to avoid interfering with the natural gait.

The pressures of the high- and low-pressure sides are recorded by two pressure transducers as shown in Fig. 2(c). The check valve in Figs. 2(a) and (c) is set to allow flow from the low- to high-pressure sides when the fluid chamber of the accumulator is empty. If chambers connected to the high-pressure side attempt to extend, the required flow through the check valve prevents negative pressure and the potential risk of air suction. For the same reason, the low-pressure oil tank is slightly pressurized to 2 to 3 bar.

Rotary valves have been proven to have high dynamic response and low power consumption [19]. Fig. 2(b) shows our RCV block prototype. The RCV block contains two 4-port 3-position directional control valves, two 3-port 2-position directional control valves, two pressure transducers, and a check valve. As shown in Fig. 2(c), the RCV block is highly compact and has six units to control the connection of six chambers. The outline dimensions of the RCV block are $40 \times 144 \times 110$ mm (length \times width \times height). Even though a small-size RCV, the equivalent diameter of the minimum orifice is 6 mm, to achieve sufficient flow capacity. As shown in Fig. 2(d), through the four-bar linkage, the steering motor (model 139885 from Maxon Ltd, Switzerland) outside the housing can actuate the inner cage nested in the outer cage as shown in Fig. 2(e). All the contact surfaces between rotary cages are well-honed and matched to reduce friction and leakage. The Oldham couplings are set to tolerate the error of coaxiality and concentricity, and thus the resistance of rotary cages is low. Therefore, the rotary load is substantially attenuated so that the low-power coreless motor is adequate to shift the position

of the inner cage.

Compared to common spool valves actuated by solenoids, the RCV is more compact and lightweight. Most importantly, RCV does not need a reset spring and consumes no energy at any static stage. Due to the low mass and small inertia of the stems and inner cages, the required power of the actuator is much lower than general solenoids. In addition, under dynamic conditions, the centro-symmetric orifices contribute no flow force to the inner cage and therefore, no tangential force is applied to the rotary actuator. These designs result in low energy consumption and high responsive frequency of the RCV block.

III. MODELING AND CONTROL STRATEGY OF HYEXO

In this section, firstly, we build the dynamic model of HyExo to evaluate the interactive force between HyExo and the user. Secondly, the hydraulic pressure model is introduced and the control strategy of the optimization-based RCV switching time design is presented.

A. Force Analysis of Non-anthropomorphic Structure

For a man-machine interactive system, the interactive force between the human body and the exoskeleton should be evaluated. During the stance phase, the exoskeleton is expected to transmit the weight of the payload to the ground. During the swing phase, the stirrup is expected to apply little force on the foot so that the wearer can take a step freely. To verify the feasibility of the design and simulate its performance, the dynamical model in walking scenario is built and analyzed in this section.

As shown in Fig.3, we build the dynamic model of HyExo in the sagittal plane. To accomplish the goal mentioned above, the cylinders and the elastic elements should be set in a proper position. The springs are used for counteracting the mass of the rods and the torque produced by the cylinders during the swing phase. In Fig. 3(b), the free body diagram is protracted to analyze every rigid body. F_b and F_l are the force provided by the back cylinder and the knee cylinder. F_h and F_k are the interactive force between the backpack, upper rod, and lower

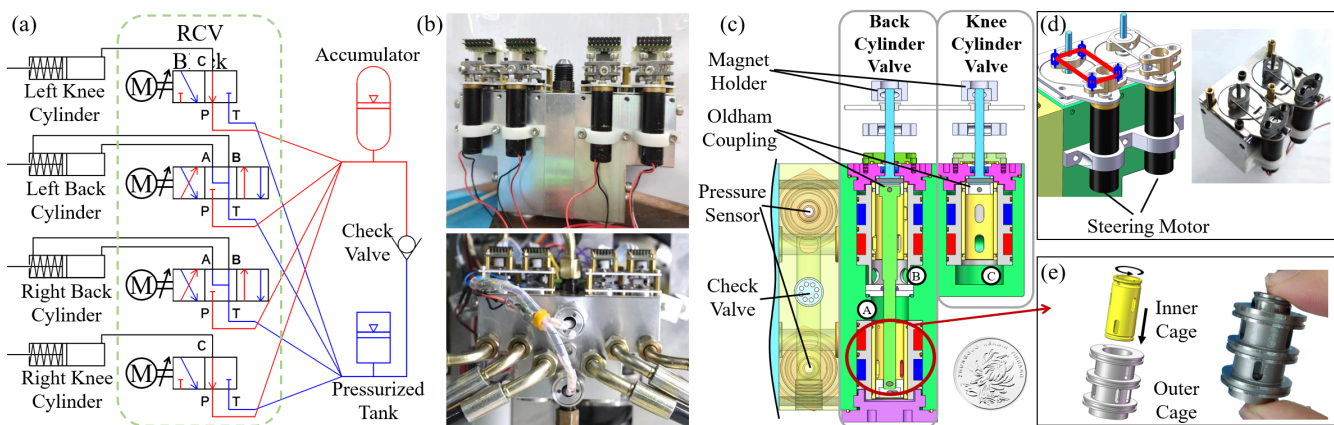


Fig. 2. (a) The hydraulic circuit of HyExo. Red lines represent high pressure, and blue lines represent low pressure. (b) The front and back view of RCV block. (c) The section view of half an RCV block. The red and blue chambers are inflated with high- and low-pressure oil, respectively. Port A and C connect to the rodless side of the back and knee cylinders, respectively, and Port B connects to the rod side of the back cylinder. (d) The four-bar steering linkage of the RCV's actuator. (e) Each pair of rotary cages consists of an inner cage (spool) and an outer cage (sleeve).

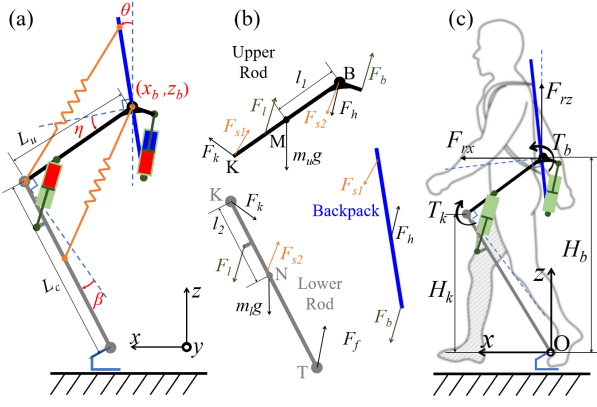


Fig. 3. The force analysis diagrams of HyExo in the sagittal plane. (a) is the definition of HyExo's degrees of freedom. (b) is the free body diagram of the three parts of the exoskeleton. (c) is the interaction diagram between the wearer and HyExo.

rod. F_f is the interactive force at TP. $m_u g$ and $m_l g$ are the gravity of the upper rod and lower rod through the center of mass. F_{s1} and F_{s2} are the pull force from springs. L_u , L_l , l_1 , and l_2 are the length of upper rod, lower rod, COM of upper rod to B, and COM of lower rod to K, respectively.

The rigid body dynamics model of one leg is established based on the Newton-Euler method [20]. For every rigid single rigid body, the dynamics can be expressed as below,

$$\begin{bmatrix} \mathbf{F} \\ |\tau| \end{bmatrix} = \begin{bmatrix} m\mathbf{I}_2 & 0 \\ 0 & I_{cz} \end{bmatrix} \begin{bmatrix} \mathbf{a}_c \\ |\alpha| \end{bmatrix}, \quad (1)$$

where $\mathbf{F} \in \mathbb{R}^2$ is the resultant vector of planar forces, and $|\tau|$ is the total torque about the center of mass. m is the mass of the rigid body, \mathbf{I}_2 is a second order identity matrix, and I_{cz} is the inertia of the rigid body at the center of mass about the z-axis. \mathbf{a}_c and α are the acceleration of the center of mass and the angular acceleration respectively. \mathbf{a}_c and α are derived from the experiment data of the real typical gait data. As shown in Fig. 3(a), the x_b and y_b are derived from the θ , η , and β of the leg in the stance phase. Meanwhile, the acceleration and angular acceleration of the legs can be derived from the joint angles. The generalized coordinates z_b , x_b , θ , η , β and their positive direction are indicated in Fig. 3(a).

Because of the low inertia of fluid transmission, the fluctuation cause by flow force is neglected and the pressure of the tanks mainly depends on the oil volume. Compared to the two main flow sources (i.e., accumulator and pressurized tank), the oil pressure inflation in the cylinder is not significant. Moreover, the cylinders and the valves transfer oils between the high- and low-pressure sides. We obtain the hydraulic pressure model as

$$\begin{cases} \text{Accumulator: } C_h = P_h V_{hg}^\gamma, V_{hg} + V_{hf} = V_h, \\ \text{Pressurized tank: } C_l = P_l V_{lg}^\gamma, V_{lg} + V_{lf} = V_l, \\ \text{Entire system: } V_{hf} + V_{lf} = C_0, \end{cases} \quad (2)$$

where C_h and C_l are constant, P_h and P_l are the pressures of the accumulator and the pressurized tank, respectively. V_{hf} (V_{hg}) and V_{lf} (V_{lg}) are the volume of the fluid (gas) in the accumulator and the pressurized tank, respectively. V_h and V_l

are the rated volume of the accumulator and the pressurized tank, respectively. γ is the heat capacity ratio of Nitrogen in adiabatic condition. C_0 represents the (constant) sum of the oil in tanks during a steady state. F_l and F_b are the hydraulic cylinder forces, and the pressure comes from the tanks.

$$\begin{cases} F_l = S_c(P_{rl} - P_{atm}) - F_f \text{sgn}(\dot{\beta}), \\ F_b = S_c P_{rl} - (S_c - S_r)P_r - S_r P_{atm} - F_{fr} \text{sgn}(\dot{\eta}), \end{cases} \quad (3)$$

where S_c is the area of the piston, and S_r is the area of the piston rod. For every cylinder, P_{rl} is the pressure of the rodless side, and P_r is the pressure of the rod side. P_{atm} is the atmospheric pressure. F_{fr} is the friction force. P_r and P_{rl} can be P_h or P_l depending on the connection of the RCV block. Due to the high flow capacity of the RCV, the pressure drop at the orifices and viscous resistance at the hose can be omitted.

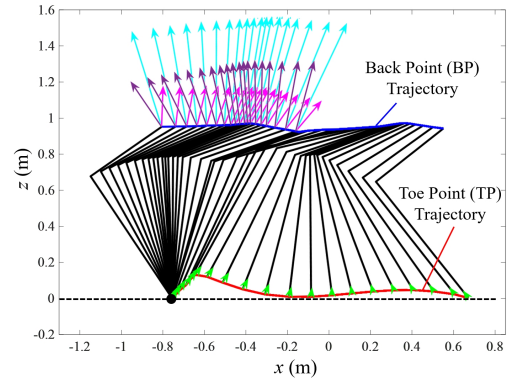


Fig. 4. The visualization of the man-machine interaction force of an entire gait cycle in simulation. Black lines are the keyframes of one leg's rods. Green arrows represent the force vectors F_f at TP during the swing phase, and cyan arrows represent the resultant force F_r , which is the sum of F_{s1} , F_h , and F_b on the backpack during the stance phase. The purple and magenta arrows represent the F_r when only the back cylinder is activated and only the knee cylinder is activated, respectively.

The angular acceleration and acceleration of the upper and lower legs are constructed in the supplementary material (S1) and (S2). Apply equation (2), (3), (S1) and (S2) into equation (1), then the man-machine interaction forces can be solved out and estimated. When the state of the exoskeleton reaches an expected stable working point, the performance of the assistance is simulated and the effect is verified. Fig.4 shows the keyframes of a time sequence whose interval is 30 ms. In the simulation, the kinematic profile of the exoskeleton was obtained from a physical experiment. In this experiment, the operator wore an apparatus to measure joint angle sequences while walking on level ground. The stiffness and the preload of the elastic element are tuned to minimize the interfering force (green vectors) during the swing phase. During the stance phase, the load force is shared by the exoskeleton substantially. The P_h is set at 1.5 MPa, and the P_l is set at 2 bar. Integrate the resultant force of the backpack, it turns out the exoskeleton spares 196 N on average during the stance phase. While during the swing phase, the average interactive force is within 17 N.

B. Hydraulic Control Strategy

For human bipedal gait, the joint trajectory is periodic and repetitive. Since the displacement and power variation of each joint is deterministic, direct hydraulic-to-hydraulic modulation is a method to fulfill regulation of the mechanical work with high flexibility and little energy loss. As a quasi-passive exoskeleton, HyExo needs to alter the valve connection to assist in carrying the load. Fig. 5(a) illustrates the coordination between human walking gait and HyExo. During the swing phase, the valve connection is in transparent mode, i.e., the cylinders are all inflated with low-pressure oil, so that HyExo's leg rods do not interfere with the wearer's legs, which increases safety and prevents stumbling.

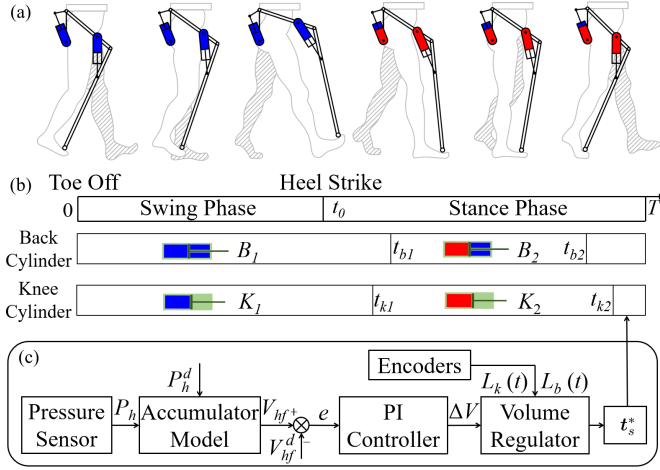


Fig. 5. The schematic diagram of the HyExo control design. (a) The coordination of the HyExo control with wearer walking gait. (b) The corresponding state (open and close) of the knee and back cylinders. B_i and K_i , $i = 1, 2$, are the state codes of different connection of cylinders. (c) The HyExo control block diagram.

The stance phase starts as the heel strikes. The operating states of the cylinders change to B_2 and K_2 to initiate assistance, as shown in Fig. 5(b). At the end of stance phase, HyExo generates a pushing force to TPs. This assistance may prevent the occurrence of toe-off. To solve this problem, the stirrup is designed to measure the toe extension angle as a trigger of the phase change. As shown in Fig. 6, the sharp rise of the toe flip angle ϵ at the end of the stance phase, also known as pre-swing [17], could be utilized as a signal to toggle the gait phase. We set a threshold of ϵ_t for the toe extension angle, beyond which the gait phase is changed. The time error before the actual phase change occurs is denoted as T_{te} , which is typically greater than the switching time of RCVs. To improve fault tolerance and safety, the rising edge of the forefoot sensor signal is also used as a trigger for phase change.

Fig. 5(c) illustrates the HyExo control design flowchart. P_h^d and V_{hf}^d are the desired pressure of the high-pressure side and the corresponding fluid volume in the accumulator, respectively. The fluid volume V_{hf}^d is calculated by the accumulator model in (2), $V_{hf}^d = V_h - (C_h/P_h^d)^{\frac{1}{\gamma}}$. At start of the stance phase, the pressure of the high-pressure side P_h is measured by the pressure sensor, and V_{hf} is derived in the same way, that is, $V_{hf} = V_h - (C_h/P_h)^{\frac{1}{\gamma}}$. The regulator

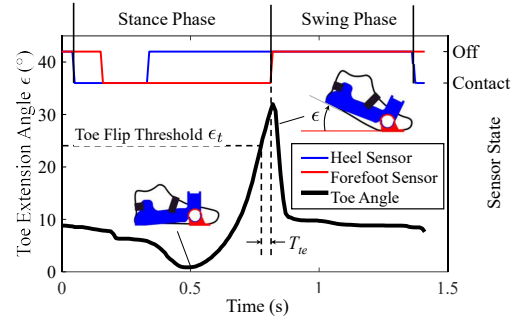


Fig. 6. In a gait cycle, the flip angle of toe joint ϵ shows a sharp increase at the end of stance phase. The heel sensor and forefoot sensor are the force sensor based on FSR shown in Fig. 1(b).

maintains a proportional-integral (PI) controller using the error $e = V_{hf} - V_{hf}^d$ as input, and ΔV is the output. ΔV is the required volume variation of the high-pressure side in each gait cycle. The volume regulator then determines the switching timings of state change of cylinders to satisfy the required ΔV .

Fig. 7 shows the variations of the cylinder lengths with human walking gait events on level ground in experiments. After the heel strike event occurs at t_0 , the knee cylinder is compressed and the back cylinder extends. The operating state of the back cylinder changes back to B_1 at $t = T$ (i.e., the end of a gait cycle) and for the knee cylinder, it changes back to K_1 at the same time. We denote the length profiles of the back and knee cylinders during one gait stride as $L_b(t)$ and $L_k(t)$, $t \in [0, T]$, respectively. We conducted these experiments to investigate the feature of the anthropomorphic gait and tune the placement of cylinders, so that the extension of the back cylinder equals to the compression of the knee cylinder during the stance phase. By doing so, it guarantees energy conservation and ΔV is zero in a level-ground gait cycle. The hydraulic control design coordinates the HyExo motion with gait phases change of human walking on different terrains. The switch timings of cylinder connections need to be planned and optimized and we discuss this in the next subsection.

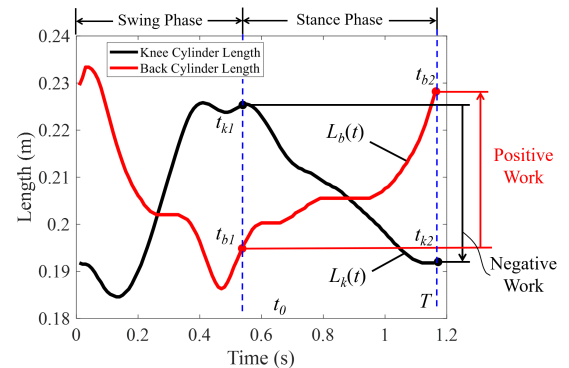


Fig. 7. The illustrative diagram of cylinder length of a knee cylinder and the ipsilateral back cylinder. The lengths of extension of the back cylinder (red line) and contraction of the knee cylinder (black line) are the same during the stance phase.

C. Optimization of RCVs' Control

As discussed previously, the back and knee cylinders are involved in the energy management and control of HyExo. The energy regulator can harvest or release energy during

the walking stance phase. We denote $t_{k1} \in [t_0, T]$ (t_{b1}) and $t_{k2} \in [t_0, T]$ (t_{b2}) with $t_{b1} < t_{b2}$, $t_{k1} < t_{k2}$ as switching times to connect (disconnect) the knee and back cylinders to high-pressure side, respectively. Here t_0 is the time moment when the stance phase starts and T is the walk stride period. Therefore, (t_{k1}, t_{k2}) and (t_{b1}, t_{b2}) are the respective time intervals of the knee and back cylinders when they are connected to the high-pressure side.

Fig. 8 illustrates how the regulator works to determine the switching times. To maximize the impulse of the vertical support force during the stance phase, the redistribution of joint energy is an optimization problem. Denoting the BP support force as $\mathbf{F}_r = [F_{rx} \ F_{rz}]^T$ (see Fig. 3(c)), the objective function $J(\mathbf{t}_s)$ is expressed as

$$J(\mathbf{t}_s) = \int_{t_0}^T F_{rz} dt, \quad (4)$$

where switching times $\mathbf{t}_s = \{t_{k1}, t_{k2}, t_{b1}, t_{b2}\}$ are the design variables to maximize $J(\mathbf{t}_s)$. As the constraint for the regulator design, the needed one-step ΔV equals the sum of the volume variations of all cylinder chambers inflated with high-pressure oil during the gait stance phase, namely,

$$-\frac{\Delta V}{S_c} = \Delta L_k + \Delta L_b, \quad (5)$$

where $\Delta L_k = L_k(t_{k2}) - L_k(t_{k1})$ and $\Delta L_b = L_b(t_{b2}) - L_b(t_{b1})$ are the knee and back cylinder variations, respectively, and S_c is the cross-sectional area of the cylinder pistons.

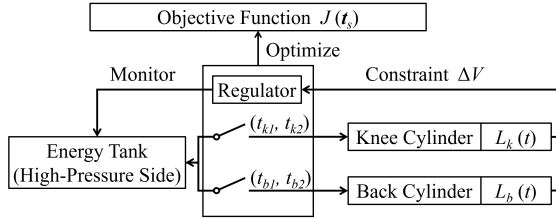


Fig. 8. The schematic of energy regulation to determine switching time \mathbf{t}_s .

To calculate the interaction forces, we use a simplified model without considering human motion dynamics. In the cartesian coordinate system, x_b and z_b are expressed as

$$\begin{cases} x_b = L_c \sin(\theta + \eta - \beta) - L_u \sin(\pi/2 - \theta - \eta), \\ z_b = L_c \cos(\theta + \eta - \beta) + L_u \cos(\pi/2 - \theta - \eta), \end{cases} \quad (6)$$

Using virtual work principle, force \mathbf{F}_r is obtained as

$$\mathbf{F}_r = \begin{bmatrix} F_{rx} \\ F_{rz} \end{bmatrix} = \begin{bmatrix} \frac{\partial x_b}{\partial \beta} & \frac{\partial x_b}{\partial \eta} \\ \frac{\partial z_b}{\partial \beta} & \frac{\partial z_b}{\partial \eta} \end{bmatrix}^{-1} \begin{bmatrix} T_k \\ T_b \end{bmatrix}, \quad (7)$$

where T_k and T_b are the torques generated by the knee and back cylinders, respectively. When the cylinders extends, T_k and T_b are positive. Using (6) and (7), we obtain

$$F_{rz} = \frac{1}{L_c L_u \cos \beta} (T_k H_b + T_b H_k), \quad (8)$$

where $H_b = L_c \cos(\theta + \eta - \beta) + L_u \sin(\eta + \theta)$, and $H_k = L_c \cos(\theta + \eta - \beta)$ are the heights of the BP and KP (see Fig. 3(c)). Due to $H_b > 0$ and $H_k > 0$, T_k and T_b contribute positively to F_{rz} . If $t_{k1} = t_{b1} = t_0$, $t_{k2} = t_{b2} = T$, that is,

$\mathbf{t}_s = \{t_0, T, t_0, T\}$, the objective function $J(\mathbf{t}_s)$ is maximized without considering constraint (5) as follows.

$$J^*(\mathbf{t}_s) = \frac{1}{L_c L_u} \int_{t_{k1}}^{t_{k2}} \frac{T_k H_b}{\cos \beta} dt + \int_{t_{b1}}^{t_{b2}} \frac{T_b H_k}{\cos \beta} dt. \quad (9)$$

To satisfy the constraint (5), we propose a method called competition of marginal benefit (CMB) to compute the optimal switching time \mathbf{t}_s^* . The marginal benefit of moving the switch timing is defined as the marginal change of mechanical work over the cost of J . There are four options to move the switch timing, increasing t_{b1} or t_{k1} positively, or decreasing t_{b2} or t_{k2} negatively. For t_{i1} and t_{i2} , $i = k, b$, their marginal benefits are

$$B_{i1} = \frac{dL_i/dt}{\partial J/\partial t_{i1}}, \quad B_{i2} = \frac{dL_i/dt}{-\partial J/\partial t_{i2}}, \quad i = k, b. \quad (10)$$

$L_k(t)$ and $L_b(t)$ are obtained from the measured data by the encoders in real time. Numerically, the derivatives of $L_k(t)$ and $L_b(t)$ in (10) are calculated. Among the above four options, the greatest one is chosen to change a time interval Δt and update switching time set \mathbf{t}_s recursively. Algorithm 1 illustrates the final optimization approach to compute \mathbf{t}_s^* .

Algorithm 1 CMB-based optimizer to compute \mathbf{t}_s^*

Input: $L_d(t)$, $L_k(t)$, t_0 , e_0 , T , Δt and ΔV .

Output: Optimal switching time set \mathbf{t}_s^*

- 1: $t_{k1} = t_{b1} = t_0, t_{k2} = t_{b2} = T, E = -\Delta L_k - \Delta L_b - \Delta V/S_c$
- 2: **while** $|E| > e_0$ and $t_{k1} < t_{k2}$ and $t_{b1} < t_{b2}$ **do**
- 3: Compute and evaluate $\{B_{k1}, B_{k2}, B_{b1}, B_{b2}\}$ at \mathbf{t}_s by (10)
- 4: **if** $E > 0$ **then**
- 5: Find minimum among $\{B_{k1}, B_{k2}, B_{b1}, B_{b2}\}$
- 6: **else**
- 7: Find maximum among $\{B_{k1}, B_{k2}, B_{b1}, B_{b2}\}$
- 8: **end if**
- 9: Update \mathbf{t}_s with the best marginal benefit. $t_{i1} \leftarrow t_{i1} + \Delta t$, or $t_{i2} \leftarrow t_{i2} - \Delta t$, $i = k$ or b .
- 10: **end while**
- 11: **return** $\mathbf{t}_s^* = \{t_{k1}, t_{k2}, t_{b1}, t_{b2}\}$

As one computational example, Fig. 9 shows the optimization results of the switching times \mathbf{t}_s for the cylinder length curves shown in Fig. 7 by the CMB method. It is clear from the figure that when $\Delta V < 0$ (energy released), $t_{k1} > t_0$, $t_{b2} = T$; when $\Delta V > 0$ (energy harvest), $t_{b2} < T$; and $t_{b1} = t_0$ and $t_{k2} = T$ for all time.

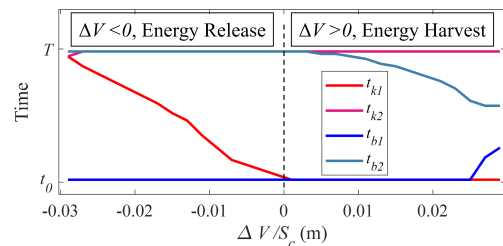


Fig. 9. The switching timing \mathbf{t}_s^* optimized by Algorithm 1 when ΔV is not zero.

IV. EXPERIMENTS AND RESULTS

A. Experiment of RCVs

We conducted closed-loop frequency response tests on RCVs to track position trajectory. The bandwidth was calculated at the cutoff frequency with -3 dB decline and the 45° phase margin. The gain-limited bandwidth is around 13.0 Hz and 14.2 Hz for the back and knee valves respectively. The phase-limited bandwidth is around 16.5 Hz for both the knee and back valves. Furthermore, by analyzing the step response results, we can obtain that the knee valve has a rise time of 31 ms, while the back valve has a slightly lower rise time of 26 ms. Considering the frequency of normal human walking gait ranges from 50 to 130 cycles per minute, the valve's responses are fast enough to be used in following human steps. For a back valve unit, a 40° switching action consumed 0.111 ± 0.005 J (mean and standard deviation) on average. For a single knee valve unit, a 60° switching action consumed 0.132 ± 0.006 J on average. In a gait cycle with period of 1.2 s, the average power consumption of the RCV block is around 0.8 W.



Fig. 10. The 6-DOFs of HyExo is demonstrated in motions such as stepping, abduction of the hip, and waist twisting.

B. Walking Experiment

A total of eight healthy subjects (age: 25.4 ± 2.4 years; weight: 75.1 ± 4.9 kg; height: 1.79 ± 0.05 m, mean and standard deviation) were recruited to participate in the walking experiments to test HyExo. All participants self-reported to be able bodied and in a good health condition. An informed consent form was signed by all the subjects and the testing protocol was approved by Medical Ethics Committee of School of Biomedical Engineering and Instrument Science at Zhejiang University (Project identification code: 2021-39). We evaluated the performance of the non-anthropomorphic design and the feasibility of the energy modulation strategy. Fig. 10 shows the donning effect of HyExo in different postures. The exoskeleton was flexible and no obvious interference was observed from the feedback of the subjects when conducting these motions.

One subject was then asked to conduct the walking tests on a treadmill. The subject accelerated from rest up to 4 km/h and then walked for 2 minutes. Both level and uphill walking tests were conducted. All onboard sensors measurements were recorded and sampled at a frequency of 100 Hz. Three sets of experiments were conducted to test the exoskeleton's load-carrying and the energy modulation performance.

- Set 1: The subject wore the exoskeleton without extra load, walked at a speed of 4 km/h for 2 minutes on level ground with the shut-down RCVs.

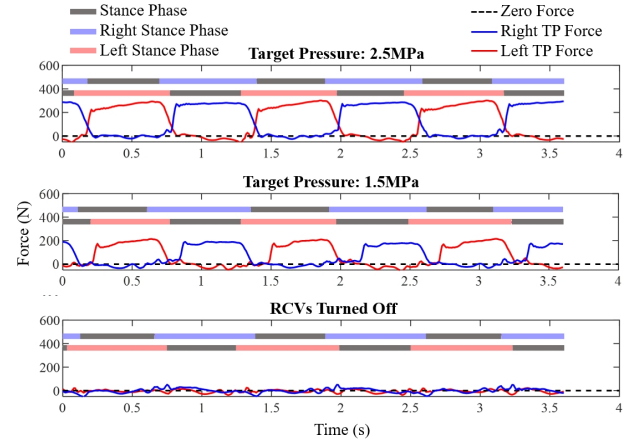


Fig. 11. The forces measured by the load cell at TP in sets 3,2 and 1. The blue, red and gray stripes are the gait phase of legs.

- Set 2: The subject wore exoskeletons without carrying additional loads and walked at a speed of 4 km/h for 2 minutes on level ground, as well as slopes of 3° , 6° , and 9° , with the RCVs turned on. The target pressure P_h^d was set at 1.5 MPa.
- Set 3: The subject wore the exoskeleton with 15kg load, walked at a speed of 4 km/h for 2 minutes on level ground with the RCVs turned on. The target pressure P_h^d was set at 2.5 MPa.

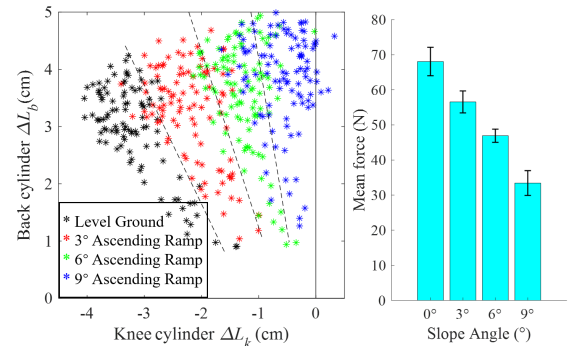


Fig. 12. (a) The length variations of the back cylinder and the knee cylinder during the stance phase. The dash lines are the hyperplane between two adjacent data sets. (b) The calculated mean force transformed to the ground by an unilateral leg during the whole gait cycle.

When P_h is stable, Fig. 11 shows the results of the force F_{TP} measured by the load cell at TPs. The load cell only measured the force parallel to its axis, the vertical load transferred to the ground can be conservatively estimated by $F_{rz} = F_{TP} \cos \epsilon$. The load supporting effect is clearly observed by the force measurements. In set 1, RCVs were shut down and during the stance phase, the exoskeletons did not provide any additional support as the toe force measurements around zero. In contrast, in set 2 and 3, with RCVs turned on, the average support force during stance phase is 169 N and 226 N respectively. HyExo provides an average support force of 136 N and 237 N throughout the entire gait cycle for P_h^d of 1.5 MPa and 2.5 MPa, respectively. Due to the inertia and mass of the upper body, the temporary absence of assistance force has little effect on the support of the load. During the swing phase, there is a slight fluctuation observed around zero in the

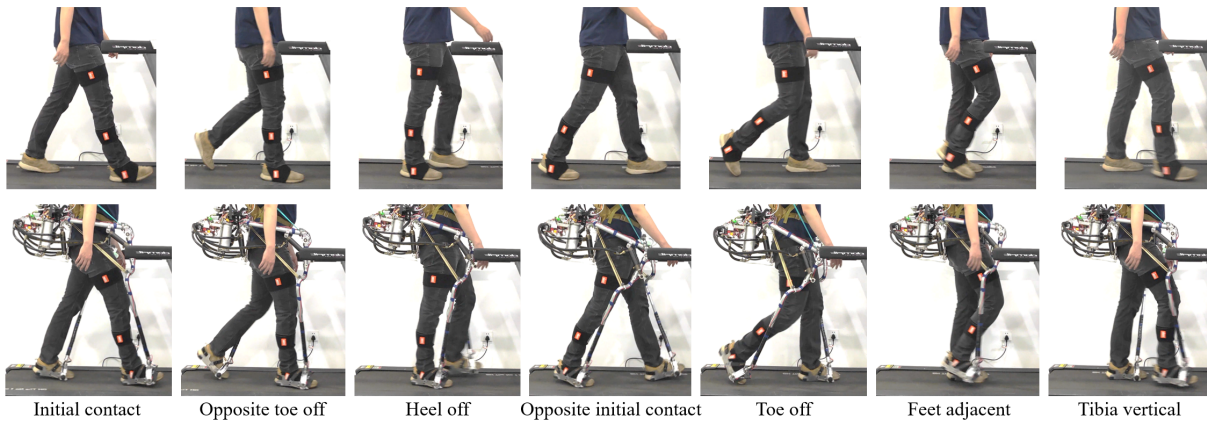


Fig. 13. Photos of a participant walking in the control group (first row) and in the HyExo-on group (second row).

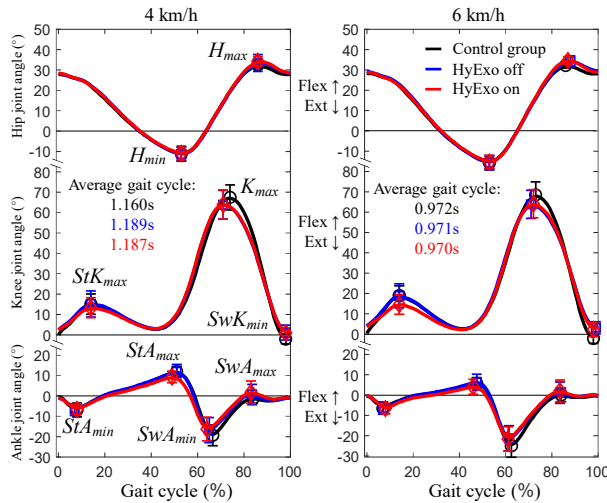


Fig. 14. The joint angle of hip, knee, and ankle averaged across participants, with the error bars of key extremum points.

TABLE I
THE STATISTIC RESULT OF THE p -VALUE IN PAIRED T-TEST BETWEEN DIFFERENT GROUPS.

Parameter	4 km/h walking speed		6 km/h walking speed			
	Control group & HyExo-off	HyExo off & HyExo-on	Control group & HyExo-on	Control group & HyExo-off	HyExo off & HyExo-on	Control group & HyExo-on
H_{min}	0.582	0.319	0.813	0.842	0.627	0.796
H_{max}	0.276	0.296	**	0.051	0.393	**
StK_{max}	0.887	*	*	0.900	***	***
K_{max}	**	0.978	*	**	0.435	**
SwK_{min}	*	0.840	***	**	0.541	***
StA_{min}	0.780	0.688	0.464	0.804	0.761	0.747
StA_{max}	0.937	**	***	0.634	***	0.109
SwA_{min}	*	0.736	**	**	0.739	**
SwA_{max}	0.281	0.185	0.190	0.309	0.269	0.173
Gait cycle	**	0.889	**	0.950	0.708	0.661

* $p < 0.05$, ** $p < 0.01$, *** $p < 0.001$

interaction force, which is the resultant effect of a combination of elastic, actuators and inertial forces. However, the force is predominantly exerted in the pull direction, which provides advantages for lifting the feet and preventing stumbling.

We collected the length variation of the back cylinder ΔL_b and that of the knee cylinder ΔL_k . Fig. 12(a) shows the $\Delta L_k - \Delta L_b$ distributions at different ramp angles in set 2. The data sets indicate a strong correlation between the slope angle and the variations of the lengths of cylinders. With increased ramp angles, the ratios of $|\Delta L_k|/|\Delta L_b|$ decreases. The data distribution also indicates that the exoskeleton operated effectively only with the terrain of a ramp angle less than 10° when ΔL_k is negative, and the energy can be harvested to maintain the pressure. Fig. 12(b) shows the force transferred to the ground (e.g., support force from HyExo) in a whole gait cycle at various ramp angles in experiment set 2. On level ground, 3° , 6° , and 9° ascending ramps, the forces (mean and standard deviation) transferred to the ground by one side of HyExo were 68.1 ± 4.1 N, 56.6 ± 3.1 N, 46.9 ± 1.9 N, and 33.4 ± 3.5 N, respectively. It is clear that the support force on level ground was largest among the other ascending ramp surfaces.

C. Gait Analysis of Wearing HyExo

HyExo is a non-anthropomorphic exoskeleton which is optimized to reduce interference with natural gait. However, its impact on human locomotion was unclear and required further investigation. We conducted gait measurement experiment to compare the gait with and without HyExo. In order to explore the effect of HyExo on gait and distinguish whether this effect comes from the non-anthropomorphic structure or from the regulation of RCVs, we conducted three walking experiments with 8 participants. In the three experiments, the first experiment was a control group without wearing HyExo; the second experiment was wearing HyExo with RCVs off; and the third experiment was wearing HyExo with RCVs on. For each participant, the backpack straps were adjusted to maintain a stationary height H_b of 1.1 m while they stood upright. We attached IMUs (MTw Awinda Wireless 3DoF Motion Tracker, Xsens, US) on the thigh, calf, and foot of the same side of participants, and collected data at 100Hz. Each experiment collected data of 10 stable steps at walking speeds of 4 km/h and 6 km/h respectively. The gait events of Toe-off and Heel-strike were detected through a method developed by Aminian et al. [21]. The joint angle was estimated and corrected using the method described in our previous work.

[22]. The photos at key states of a gait cycle are shown in Fig. 13. The averaged curves of joint angles are plotted in Fig. 14, where the error bars of key extreme points have also been plotted. Paired-sample t-test was computed and used to compare the effect of HyExo and the regulation of RCVs. In Table I, the p -value is shown and the factors that can be considered significantly different are marked with “*”s. From the analysis results we can learn that the non-anthropomorphic structure slightly improves the gait cycle at a walking speed of 4km/h, and this effect is less significant at 6km/h. The exoskeleton increases the maximum flexion angle of the hip joint, while reducing the motion amplitude of the knee joint during the swing phase. In addition, it increases the flexion angle of the knee joint during the swing phase. The load sharing effect brought by the modulation of RCV reduces the peak value of the support period of the knee and ankle joints.

D. Energy Expenditure Test

To evaluate the energy saving performance of HyExo, we conducted human experiments and measured the metabolic cost with a wearable metabolic system (model K5 from COSMED, Italy). For every subject, the energy expenditure test consisted of six stages in random order: 1) wearing HyExo with no extra load, and the target pressure is 1.5 MPa; 2) wearing HyExo with a load of 15 kg, and the target pressure is 2.5 MPa; 3) wearing HyExo with a load of 30 kg, and the target pressure is 3.5 MPa; 4) wearing nothing without any load; 5) wearing a regular backpack weighing 15 kg; and 6) wearing a regular backpack weighing 30 kg. During the whole test, the subject walked on a treadmill at a speed of 4 km/h. Each stage lasted 6 minutes. Between any two stages, a 3-minute break was taken by the subject to have a rest and change the load. The metabolic cost was recorded for the last 2 minutes of each stage. Before and after the experiment, the subjects rested for 5 minutes and their metabolic consumption was recorded while they were not exercising. Fig.15 shows the net energy cost at each stage for all 8 subjects. Paired-sample t-test was computed and used to evaluate the effect of HyExo and determine its significance. In analysis, the statistically significant difference was defined as $p < 0.05$. Compared to a regular backpack, HyExo achieved a reduction of metabolic cost of $7.8 \pm 2.6\%$ with a load of 30 kg. However, under conditions with no additional weight and a load of 15kg, HyExo increased metabolic energy consumption by $20.5 \pm 4.1\%$ and $4.6 \pm 4.0\%$ respectively. In our experiment, the trend of metabolic cost of HyExo groups shows its advantage in carrying heavier loads. As shown in Fig.15, as the load increases, the growth rate of energy consumption in the HyExo group k_2 is lower than that of the group without HyExo k_1 .

V. DISCUSSION

The first prototype of HyExo shows its advantages in the aspects of energy consumption and load-carrying effect. The total electric energy consumption of HyExo is 1.55 W (0.8 W for the drive of the RCV block and 0.75 W for other MCUs and sensors). Table II lists major specifications of a few commercial state-of-the-art valves. Compared with other similar developed products, although it does not fully

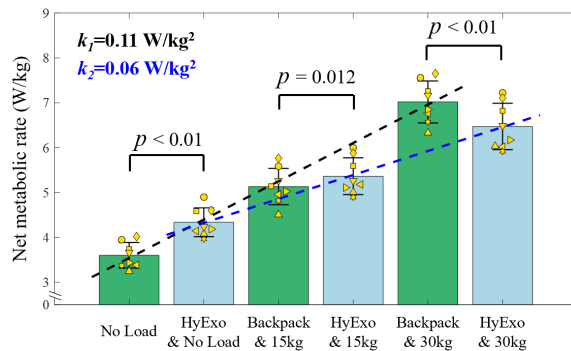


Fig. 15. The metabolic cost (mean and standard deviation) of 8 subjects at six different testing stages. The markers with different shapes indicate every participant. The dashed lines indicate the increasing trend of metabolic rate with the increase of load. k_1 and k_2 are the slope of the linear regression result.

exceed all specifications, the proposed RCV has huge advantages especially for passive-legged exoskeletons. For example, compared to the nozzle-flapper servo valves such as Moog 24 [23], the RCV achieves multi-stage function and has less leakage and much higher rated flow of 30 L/min. Compared to the direct drive valves such as Moog D638 [23], the RCV has lower power consumption and less weight. The high flow rate and low internal leakage guarantee low hydraulic energy loss. We also plan to introduce damping characteristics to reduce force fluctuation as the RCV switches. In summary, the lightweight RCV has a low power consumption and a fast response so that it can be used in exoskeletons.

To comprehensively evaluate the energy consumption, supporting capacity, and speed of the legged systems, we compare multiple exoskeletons by a metric $Q = FV/P$, where F is the mean support force, V is the speed of ambulation, and P is the corresponding power. Q is derived from the energy cost of transport (COT), defined as $COT \triangleq P/mgv$, which quantifies the energy efficiency of transporting an animal or vehicle from one place to another [24]. Here Q is the reciprocal of COT, and the mg is substituted to the average supporting force F because exoskeletons are auxiliary equipment used to share the load force rather than walk automatically. Table III lists key specifications of several state-of-the-art exoskeletons that were similarly developed for load-carrying augmentation. The metric Q was calculated for these exoskeletons. Most active and quasi-passive exoskeletons have smaller Q values than that of HyExo. This is mainly due to HyExo's low power consumption. Among other quasi-passive exoskeletons, HyExo gets highest score. Moreover, HyExo's load-supporting performance has a large room for improvement. A higher pre-charged pressure in the accumulator or a larger P_h^d would help HyExo provide greater support force than was demonstrated in the experiments. The natural gait of the human body exhibits high energy efficiency, making it difficult to lower the metabolic cost without external energy input. Most quasi-passive exoskeleton increases the users' metabolic cost [4], [25]. In this work, HyExo increased metabolic energy expenditure in the weightless and 15 kg load tests but decreased it in the 30 kg load test. HyExo slows down the rate at which metabolic cost increases with load. Using a linear regression model, it can be inferred that the reduction in energy

TABLE II
COMPARISON WITH REPRESENTATIVE PRODUCTS

Product	Principle	Weight	Rated Flow	Energy Consumption	Response	Leakage
Rexroth NG6 (e.g., RE 23164)	Spool valve	1.6 kg	60 L/min@7 bar	26 W	Switching time 20-45 ms, maximum switching frequency 15000/h	-
MOOG G773	Nozzle flapper	0.86 kg	57 L/min@35 bar	0.064 W	Step response time of 100% stroke: 17 ms	<1.9 L/min
Domin S6 Pro	Rotary-linear	0.55 kg	60 L/min@70 bar	less than 5 W	Frequency Response: (-3 dB gain, $\pm 25\%$ signal) 190 Hz; Step Response: < 3.5 ms	<1.1 L/min @100 bar
Proposed RCV valve	Rotary cage	0.35 kg	30 L/min@7 bar	16 V, mean power 0.2 W	14 Hz (-3 dB gain, $\pm 25\%$ stroke)	<0.06 L/min

expenditure begins to manifest at approximately 18.4 kg of load. This is mainly due to its self weight and potential internal leakage in the hydraulic circuit, which limits the efficiency of energy recovery. The weight of HyExo can be further reduced by replacing the heavy off-the-shelf components with customized ones. The leakage can be reduced by improving the sealing method. In terms of safety, HyExo has no power source for joint actuation, and the output energy thus could not exceed the power exerted by the wearer, which makes it safer than actively actuated exoskeletons.

TABLE III
COMPARISON OF LOAD-SUPPORTING EXOSKELETONS

Study	Speed (km/h)	Mean Support Force (N)	Power (W)	Q (kmN/W/h)
This work	4	237	1.6	592.5
Yang <i>et al.</i> [26] (2022)	1.08	73.3*	-	-
Leng <i>et al.</i> [27] (2021)	5	80	24.7	16.2
Xiang <i>et al.</i> [28] (2021)	2.88	110	-	-
Zhou <i>et al.</i> [29] (2021)	3.5	38.1*	0	-
Khazoom <i>et al.</i> [12] (2020)	5	293	84	17.4
Wang <i>et al.</i> [30] (2020)	2	441	-	-
Hao <i>et al.</i> [13] (2020)	2.5	83.8	4.9	42.8
Dijk <i>et al.</i> [5] (2018)	5.7	130	-	-
Gregorczyk <i>et al.</i> [31] (2010)	4.8	182.1*	-	-
Ikeuchi <i>et al.</i> [32] (2009)	5.7	130	-	-
Walsh <i>et al.</i> [25] (2007)	3.3	225.8*	2	372.6
Zoss <i>et al.</i> [33] (2005)	4.7	735	2270	1.5

* The data is inferred from the literature, see supplementary Table S1 for details.

VI. CONCLUSION

This paper presented HyExo, an RCV-based novel non-anthropomorphic exoskeleton to transmit the load force from the back to the ground. Under the CMB-based energy modulation strategy, HyExo achieved remarkable load-supporting performance in the experiments. HyExo demonstrates a slower increase in metabolic energy expenditure as the load is increased, and achieves a reduction of metabolic cost carrying heavy load. This work verifies the possibility of controlling energy flow among joints without prime movers (motor and pump) and only using lightweight quasi-passive hydraulic components (RCVs) to achieve load-bearing enhancement. HyExo's low energy consumption makes it possible for more outdoor scenarios. Future work will focus on the detection and prediction of complex, changeable terrains, which may contribute to long-time hiking in the field.

REFERENCES

- [1] H. Kim, Y. J. Shin, and J. Kim, "Design and locomotion control of a hydraulic lower extremity exoskeleton for mobility augmentation," *Mechatronics*, vol. 46, pp. 32–45, 2017.
- [2] N. D. Manring and R. C. Fales, *Hydraulic Control Systems*, 2nd ed. New York, NY: John Wiley & Sons Inc., 2019.
- [3] A. Zoss and H. Kazerooni, "Architecture and hydraulics of a lower extremity exoskeleton," in *Proc. ASME Int. Mech. Eng. Cong. Expo.*, Orlando, FL, 2005, pp. 1447–1455.
- [4] K. N. Gregorczyk, L. Hasselquist, J. M. Schiffman, C. K. Bensek, J. P. Obusek, and D. J. Gutekunst, "Effects of a lower-body exoskeleton device on metabolic cost and gait biomechanics during load carriage," *Ergonomics*, vol. 53, no. 10, pp. 1263–1275, 2010.
- [5] W. van Dijk, T. Van de Wijdeven, M. Holscher, R. Barents, R. Könemann, F. Krause, and C. Koerhuis, "Exobuddy - a non-anthropomorphic quasi-passive exoskeleton for load carrying assistance," in *Proc. IEEE Int. Conf. Biomed. Robot. Biomechat.*, Twente, Netherlands, 2018, pp. 336–341.
- [6] T. Zhou, C. Xiong, J. Zhang, W. Chen, and X. Huang, "Regulating metabolic energy among joints during human walking using a multi-articular unpowered exoskeleton," *IEEE Trans. Neural Syst. Rehab. Eng.*, vol. 29, pp. 662–672, 2021.
- [7] Y. Chang, W. Wang, and C. Fu, "A Lower Limb Exoskeleton Recycling Energy From Knee and Ankle Joints to Assist Push-Off," *ASME J. Mechanisms Robot.*, vol. 12, no. 5, 05 2020, 051011. [Online]. Available: <https://doi.org/10.1115/1.4046835>
- [8] C. Wang, L. Dai, D. Shen, J. Wu, X. Wang, M. Tian, Y. Shi, and C. Su, "Design of an ankle exoskeleton that recycles energy to assist propulsion during human walking," *IEEE Trans. Biomed. Eng.*, vol. 69, no. 3, pp. 1212–1224, 2022.
- [9] T. Li, L. Wang, J. Yi, Q. Li, and T. Liu, "Reconstructing walking dynamics from two shank-mounted inertial measurement units," *IEEE/ASME Trans. Mechatronics*, vol. 26, no. 6, pp. 3040–3050, 2021.
- [10] S. Chen, T. Han, F. Dong, L. Lu, H. Liu, X. Tian, and J. Han, "Precision interaction force control of an underactuated hydraulic stance leg exoskeleton considering the constraint from the wearer," *Machines*, vol. 9, no. 5, 2021, article 96.
- [11] H. Li, D. Sui, H. Ju, Y. An, J. Zhao, and Y. Zhu, "Mechanical compliance and dynamic load isolation design of lower limb exoskeleton for locomotion assistance," *IEEE/ASME Trans. Mechatronics*, vol. 27, no. 6, pp. 5392–5402, 2022.
- [12] C. Khazoom, P. Caillouette, A. Girard, and J.-S. Plante, "A supernumerary robotic leg powered by magnetorheological actuators to assist human locomotion," *IEEE Robot. Automat. Lett.*, vol. 5, no. 4, pp. 5143–5150, 2020.
- [13] M. Hao, J. Zhang, K. Chen, H. Asada, and C. Fu, "Supernumerary Robotic Limbs to Assist Human Walking With Load Carriage," *Journal of Mechanisms and Robotics*, vol. 12, no. 6, p. 061014, 07 2020. [Online]. Available: <https://doi.org/10.1115/1.4047729>
- [14] J. Kim, G. Lee, R. Heimgartner, D. Arumukhom Revi, N. Karavas, D. Nathanson, I. Galiana, A. Eckert-Erdheim, P. Murphy, D. Perry, *et al.*, "Reducing the metabolic rate of walking and running with a versatile, portable exosuit," *Science*, vol. 365, no. 6454, pp. 668–672, 2019.
- [15] W. Fan, T. Liu, J. Yi, X. Huang, B. Zhang, X. Zhang, and S. Wang, "A passive hydraulic auxiliary system designed for increasing legged robot payload and efficiency," in *Proc. IEEE Int. Conf. Robot. Autom.*, Xi'an, China, 2021, pp. 3097–3103.
- [16] T. W. P. Huang and A. D. Kuo, "Mechanics and energetics of load carriage during human walking," *J. Exp. Biol.*, vol. 217, no. 4, pp. 605–613, 2014.
- [17] M. W. Whittle, *Gait Analysis: An Introduction*, 4th ed. Elsevier Ltd., 2007.
- [18] J. Zhang, J. Bao, D. Zhang, B. Xu, and Q. Chao, "Inlaid connection of carbon fibre reinforced plastic cylinder," in *Proc. IEEE Int. Conf. Airc. Util. Syst.*, Beijing, China, 2016, pp. 1024–1029.

- [19] C. Yuan, A. Plummer, and M. Pan, "Switching characteristics of a high-speed rotary valve for switched inertance hydraulic converters," *Proceedings of the Institution of Mechanical Engineers, Part I: Journal of Systems and Control Engineering*, vol. 236, no. 7, pp. 1421–1441, 2022.
- [20] H. Hahn, *Rigid body dynamics of mechanisms: 1 theoretical basis*. Springer Science & Business Media, 2013.
- [21] K. Aminian, B. Najafi, C. Büla, P.-F. Leyvraz, and P. Robert, "Spatio-temporal parameters of gait measured by an ambulatory system using miniature gyroscopes," *J. Biomech.*, vol. 35, no. 5, pp. 689–699, 2002.
- [22] L. Wang, Y. Sun, Q. Li, and T. Liu, "Estimation of step length and gait asymmetry using wearable inertial sensors," *IEEE Sensors J.*, vol. 18, no. 9, pp. 3844–3851, 2018.
- [23] (2022) Moog servo valves. [Online]. Available: <https://www.moog.com/markets>
- [24] V. Radhakrishnan, "Locomotion: dealing with friction," *Proceedings of the National Academy of Sciences*, vol. 95, no. 10, pp. 5448–5455, 1998.
- [25] C. J. Walsh, K. Endo, and H. Herr, "A quasi-passive leg exoskeleton for load-carrying augmentation," *Int. J. Humanoid Robot.*, vol. 4, no. 3, pp. 487–506, 2007.
- [26] P. Yang, H. Yan, B. Yang, J. Li, K. Li, Y. Leng, and C. Fu, "A centaur system for assisting human walking with load carriage," in *2022 IEEE/RSJ International Conference on Intelligent Robots and Systems (IROS)*, 2022, pp. 5242–5248.
- [27] Y. Leng, X. Lin, G. Huang, M. Hao, J. Wu, Y. Xiang, K. Zhang, and C. Fu, "Wheel-legged robotic limb to assist human with load carriage: An application for environmental disinfection during COVID-19," *IEEE Robot. Automat. Lett.*, vol. 6, no. 2, pp. 3695–3702, 2021.
- [28] Y. Xiang, X. Yan, H. Su, N. Chen, S. Guo, J. Wu, Y. Leng, and C. Fu, "Powered super tail: A terrain-adaptive wheel-legged robotic limb to assist human's load carriage," in *2021 27th International Conference on Mechatronics and Machine Vision in Practice (M2VIP)*, 2021, pp. 676–681.
- [29] Z. Zhou, W. Chen, H. Fu, X. Fang, and C. Xiong, "Design and experimental evaluation of a non-anthropomorphic passive load-carrying exoskeleton," in *2021 6th IEEE International Conference on Advanced Robotics and Mechatronics (ICARM)*, 2021, pp. 251–256.
- [30] T. Wang, Y. Zhu, T. Zheng, D. Sui, S. Zhao, and J. Zhao, "Palexo: A parallel actuated lower limb exoskeleton for high-load carrying," *IEEE Access*, vol. 8, pp. 67 250–67 262, 2020.
- [31] J. M. S. C. K. B. J. P. O. Karen N. Gregorczyk, Leif Hasselquist and D. J. Gutekunst, "Effects of a lower-body exoskeleton device on metabolic cost and gait biomechanics during load carriage," *Ergonomics*, vol. 53, no. 10, pp. 1263–1275, 2010. [Online]. Available: <https://doi.org/10.1080/00140139.2010.512982>
- [32] Y. Ikeuchi, J. Ashihara, Y. Hiki, H. Kudoh, and T. Noda, "Walking assist device with bodyweight support system," in *2009 IEEE/RSJ International Conference on Intelligent Robots and Systems*, 2009, pp. 4073–4079.
- [33] A. Zoss, H. Kazerooni, and A. Chu, "On the mechanical design of the Berkeley lower extremity exoskeleton (BLEEX)," in *Proc. IEEE/RSJ Int. Conf. Intell. Robot. Syst.*, Edmonton, Canada, 2005, pp. 3465–3472.



Wu Fan received the B.S. degree in mechatronic engineering, in 2019, from Zhejiang University, Hangzhou, China, where he is currently working toward the Ph.D. degree in mechatronic engineering with the State Key Laboratory of Fluid Power and Mechatronic Systems, School of Mechanical Engineering.

His research interests include legged robots, weight-bearing exoskeletons and intelligent prosthetic joints.



Zhe Dai received his B.S. degree in mechatronic engineering from Zhejiang University, Hangzhou, China in 2022, and he is currently working toward the M.S. degree in mechatronic engineering at the State Key Laboratory of Fluid Power and Mechatronic Systems, School of Mechanical Engineering.

His research interests include legged robots, weight-bearing exoskeletons and bipedal robots.



Bin Zhang received the B.S. degree from Shandong University of technology, Zibo, China, in 2014, and received M.Eng. degree from the School of Mechanical Engineering, China Jiliang University, Hangzhou, China, in 2017 and Ph.D. degree in engineering from Zhejiang University, Hangzhou, China, in 2022.

His current research interests include wearable exoskeleton, the energy conversion mechanism of human lower limb for walking, and machine learning based analysis and optimization.



Long He received the B.S. degree and the M.S. degree in mechanical design and manufacturing and automation from Nanjing University of Science and Technology, Nanjing, China, in 2001 and in 2013, respectively.

He is currently a professorate senior engineer at Hangzhou ZhiYuan Research Institute. His current research interests include wearable exoskeleton, ergonomics, and human-machine interaction.



Min Pan is a reader in the Department of Mechanical Engineering at the University of Bath, UK. She was awarded her Ph.D. from the University of Bath in 2012. She was an assistant professor in the School of Mechanical Engineering at Zhejiang University in 2014 and 2015. She is currently a Leverhulme Research Fellow. Her research areas include smart fluid power actuation and control, numerical modelling of dynamic systems, control systems, and robotics.



Jingang Yi (Senior Member, IEEE) received the B.S. degree in electrical engineering from Zhejiang University, Hangzhou, China, in 1993, the M.Eng. degree in precision instruments from Tsinghua University, Beijing, China, in 1996, and the M.A. degree in mathematics and the Ph.D. degree in mechanical engineering from the University of California, Berkeley, CA, USA, in 2001 and 2002, respectively. He is currently a Professor of mechanical engineering at Rutgers University. His research interests include autonomous robotic systems, dynamic systems and control, mechatronics, automation science and engineering, with applications to biomedical systems, civil infrastructure and transportation systems.

Dr. Yi is a Fellow of the American Society of Mechanical Engineers (ASME). He currently serves as a Senior Editor of the IEEE ROBOTICS AND AUTOMATION LETTERS and as an Associate Editor for International Journal of Intelligent Robotics and Applications. He served as an Associate Editor for IEEE TRANSACTIONS ON AUTOMATION SCIENCE AND ENGINEERING, IEEE/ASME TRANSACTIONS ON MECHATRONICS, IEEE ROBOTICS AND AUTOMATION LETTERS, IFAC Journal Mechatronics, IFAC Control Engineering Practice, and ASME Journal of Dynamic Systems, Measurement and Control.



Tao Liu (Senior Member, IEEE) received the B.S. degree in mechanical engineering from the Harbin University of Science and Technology, Harbin, China, in 2001, the M.Eng. degree in mechanical engineering from the Harbin Institute of Technology, Harbin, China, in 2003, and the D.Eng. degree in intelligent mechanical engineering from the Kochi University of Technology, Kochi, Japan, in 2006. From 2009 to 2013, he was an Assistant Professor with the Department of Intelligent Mechanical Systems Engineering, Kochi University of Technology.

He is currently a Professor with the State Key Laboratory of Fluid Power and Mechatronic Systems and the School of Mechanical Engineering, Zhejiang University, Hangzhou, China. His current research interests include wearable sensor systems, rehabilitation robots, biomechanics, and human motion analysis. He was the Recipient of the Japan Society of Mechanical Engineers (JSME) Encouragement Prize, in 2010.

Responses to the Reviewers

Response to the Senior Editor and Technical Editor

We thank the senior editor and the technical editor for their constructive suggestions to improve the quality of the paper. Below, we outline the reviewers' comments and our point-by-point responses. We believe that our responses effectively address the concerns raised by the reviewers and contribute to an enhanced quality of the paper. We earnestly hope that our manuscript will merit consideration for publication after this revision.

- 1. Senior Editor's Comment: The paper has been improved according to the reviewers' comments; however, the scientific contribution is still unclear. The authors should address all comments provided by the TE and reviewers to clarify the effectiveness.**
- 2. Technical Editor's Comment: This is a resubmitted version, while three reviewers agreed the great improvement from their original version, two reviewers commented that the changes are insufficient to guarantee an acceptance. This TE concurred to their suggestions and request a Major Revision from the authors to address these concerns, in particular, those from the second reviewer.**

In this major revision, we have extended the comparison and investigated some products on the market. The effectiveness of HyExo was explained to reviewers in terms of load-bearing effect, safety, metabolic cost, etc., and questions about the experimental results were answered.

Response to Reviewer # 1

#1.1 WHAT ARE THE CONTRIBUTIONS OF THIS PAPER: The author proposes a new type of hydraulic exoskeleton, and designs a suitable hydraulic system without prime mover. The overall performance level is good.

Thanks for your positive comments.

#1.2 WHAT ARE SOME WAYS IN WHICH THE PAPER COULD BE IMPROVED: The author has well verified the advantages of the proposed exoskeleton through experiments, but the comparison with other common equipment indicators in the market is lacking, and it is hoped that the author can provide additional information.

We greatly appreciate your insightful proposal to compare exoskeleton metrics with other common devices on the market. We have carefully considered your suggestions and are seeking to enhance our work by providing more information in this regard.

In the previous revision, we have added several state-of-the-art works to Table S1 in the supplementary material and Table III in the manuscript, but most of them are concentrated in the scientific research field and are experimental prototypes.

Based on your opinions, we have added some information about products in the market and our perspective on them in **Table S2** in the supplementary file. It should be pointed out that this work involves a non-anthropomorphic weight-bearing exoskeleton, i.e., transferring the load force to the ground directly, and thus our research scope only includes lower-limb exoskeletons or supernumerary legs with similar functions, and does not include some typical and well-known ones that assist specific joints. In terms of functionality, this survey is primarily focused on human augmentation rather than rehabilitation.

However, not all exoskeletons have disclosed the key performance indicators we want to use for comparison, and the testing methods and criteria for their performance indicators also vary. Therefore, we have only selected works that have comparable features and included them in Table III of the manuscript. We hope you can agree with our approach.

From the investigation, it can be seen that most of the exoskeletons on the market are passive because commercial products need a structure as simple as possible to guarantee reliability and reduce failure rate. There are also special function exoskeletons for industry applications. Most passive exoskeletons can support loads in static positions but have difficulty providing support throughout the entire gait cycle during the dynamic walking process. This is right the focal point of our work, and we believe that our efforts will yield a novel and effective load-bearing method with lower energy consumption for the exoskeleton field. In the future, with further optimization of materials, actuation, and control, better performance can be achieved.

Due to the 11-page limit of the major revision, we have not included all of these points in the manuscript. If the manuscript meets the standards for acceptance, we will summarize and discuss these points in the 12-page final version. I hope you can agree to our plan.

We thank Reviewer 1 for his/her constructive comments and suggestions.

Response to Reviewer # 2

#2.1 WHAT ARE THE CONTRIBUTIONS OF THIS PAPER: This paper proposed a quasi-passive hydraulic exoskeleton, HyExo, built using a lightweight rotary cage valve (RCV) block that offers a fast response and low energy consumption. An optimization-based regulator is presented for joint energy distribution. The novel non-anthropomorphic structure's interaction force model and control are demonstrated and verified. The experimental study involving human subjects showed the load-supporting effect's effectiveness.

Thanks for the positive comments.

#2.2 WHAT ARE SOME WAYS IN WHICH THE PAPER COULD BE IMPROVED:
Please refer to the below comments to further improve the paper.

#2.2-1 The authors failed to offer a lucid response to the reviewer's inquiries, specifically with regard to question #2.2-1. They omitted to specify the new papers referenced and did not indicate the location in the paper where these references were made.

Thanks for your suggestion. We list the state-of-the-art works and products in Table S1 and Table S2 in the supplementary file. Additionally, the features of some comparable works in recent year are added and marked in Table III of the manuscript. It should be pointed out that this work involves a non-anthropomorphic weight-bearing exoskeleton, i.e., transferring the load force to the ground directly, and thus our research scope only includes lower-limb exoskeletons or supernumerary legs with similar functions, and does not include some typical and well-known ones that assist specific joints. In terms of functionality, the survey in Table S1 and Table S2 is primarily focused on human augmentation rather than rehabilitation.

We hope these measures address your concerns.

#2.2-2 What caused the HyExo to exhibit a decrease in metabolic cost within the 30kg payload group? The alteration in the trends of slopes K1 and K2 in light of the new results necessitates further clarification. Please provide an explanation for this phenomenon.

Thanks for your concern. In the experimental setup, the target pressure of the hydraulic system P_h^d increases linearly as the load increases. According to the data in the walking experiment, each increase in pressure of 1 Mpa can increase the support force by approximately 101 N ($237 - 136 = 101$ N). In the 30kg-payload group, HyExo exerted a larger support force due to the higher P_h^d , which decreased the metabolic energy expenditure of subjects.

In the first submission, the energy expenditure test consists of the no-load group and the 15kg-load group. In the last revision, we reconducted the experiment and added the 30kg-load groups. The alteration in the trends of slopes k1 and k2 you mentioned may refer to k1 changing from 0.12 to 0.11, and k2 changing from 0.07 to 0.06. Below is our clarification of this change.

For every subject, we denote the increasing rate of metabolic energy expenditure with load as $k_{i,j}$, $i \in \{1, 2\}$, $j \in \{1, 2, \dots, 8\}$, $i = 1$ represents group with regular backpack, and $i = 2$ represents group with HyExo, and j represents every subject.

For the experiment of the first submission, $k_{i,j}$ is derived from the metabolic costs of 15kg-load group and no-load group as below:

$$k_{i,j} = (C_{i,j,15} - C_{i,j,0})/15, \quad (R1)$$

where $C_{i,j,l}$ is the metabolic cost of the j th subject carrying l load under i condition.

For the experiment of last revision, we add an apostrophe ''' to all symbols in order to distinguish them with the data in the first submission. For the j th subject, $k'_{i,j}$ is the slope of the data in the

no-load, 15kg, 30kg groups calculated by the least square method as below:

$$k'_{i,j} = \frac{\sum_{l=0,15,30} (C'_{i,j,l} - \bar{C}'_{i,j})(l - (0 + 15 + 30)/3)}{\sum_{l=0,15,30} (l - (0 + 15 + 30)/3)^2}, \quad (\text{R2})$$

where $\bar{C}'_{i,j} = (C'_{i,j,0} + C'_{i,j,15} + C'_{i,j,30})/3$, is the average of metabolic cost with three different sets of weight. We hypothesize that the escalating rates $k_{i,j}$ among subjects follow a normal distribution, and sample $k_{i,j}$ and sample $k'_{i,j}$ are drawn from the same distribution. We plot the probability density function of the distributions fitted from $k_{1,j}$, $k_{2,j}$, $k'_{1,j}$, and $k'_{2,j}$ in Fig. R1. Additionally, a paired-sample t-test was performed to assess the significance of the disparity between $k_{i,j}$ and $k'_{i,j}$. The resulting p-values exceed 0.05, indicating that the proposition that $k_{i,j}$ and $k'_{i,j}$ emanate from the same distribution cannot be dismissed.

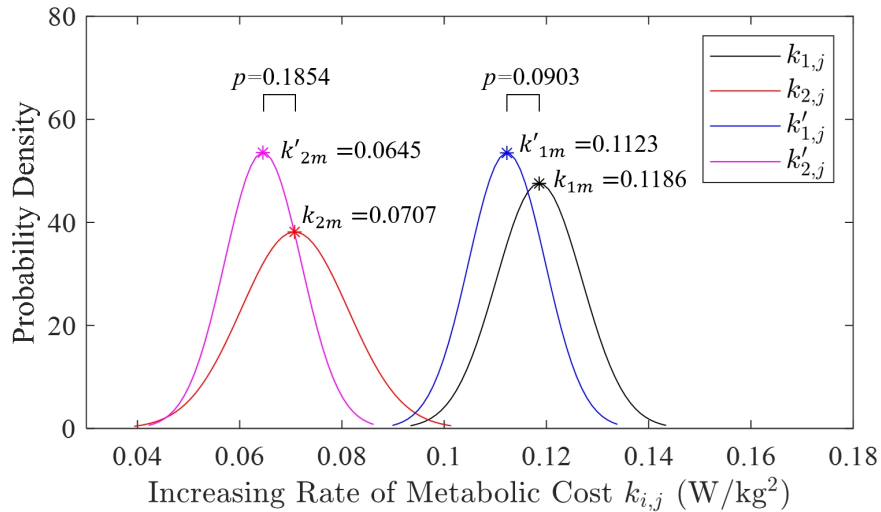


Figure R1: The probability density function of the possible distribution fitted from the samples of $k_{1,j}$, $k_{2,j}$, $k'_{1,j}$, and $k'_{2,j}$. The subscript m indicates mean among subjects.

To sum up, the k values were rounded to two decimal places, which increases the error from the experimental results of the first submission. Nonetheless, based on the t-test results, we can still infer that the k values originate from the same distribution.

We speculate that the reasons for the difference in k values between the two experiments may be the season and the introduction of 30kg-load groups. The first experiment was carried out in April, while the second one took place in August. Differences in temperature and the subjects' clothing may have contributed to the alteration in k values. Furthermore, since the second experiment introduced 30kg-load groups, this set of data affected the k value. Although some studies have shown that the rate of metabolic energy expenditure increases approximately linearly with load [1], but may not be strictly linear. We have employed a linear model to fit the trend of metabolic cost, which may cause k values to be affected slightly when 30kg-load groups are introduced.

Although there is a small fluctuation in the k value, we draw the same conclusion, that is, HyExo can slow the increasing rate in metabolic cost as load increases.

#2.2-3 Referring to Table R1, it appears that the safety aspect is conspicuously absent from the listed features of the proposed work. Considering that exoskeletons are worn by humans, safety is arguably a fundamental and critical feature. Could you kindly provide an explanation for this omission?

Thank you for your insightful suggestion. Safety is indeed one of the key issues that need to be considered in exoskeletons. However, there are hardly any examples of large-scale commercial applications of active exoskeletons by far, and there are no reports of relevant safety accidents. It is difficult to evaluate the safety of these hydraulic drive methods from the actual case level. Besides actuation, safety also depends on the sensing system, control system, and mechanical structure, so the safety cannot be judged just through actuation. Nonetheless, we can still analyze the potential hazards of several actuation schemes in Table R1 from the aspects of power source and transmission characteristics as follows:

(a) Pump Driven System

The system pressure is affected by the motor power and the relief valve. Control system error and failure of the direction control valve may cause the exoskeleton joints to generate uncontrolled huge torque, which may injure the wearer.

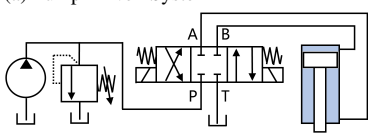
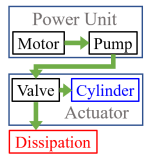
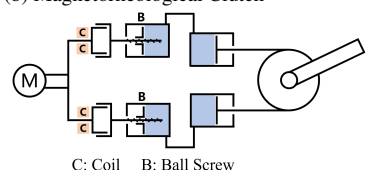
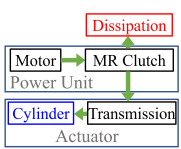
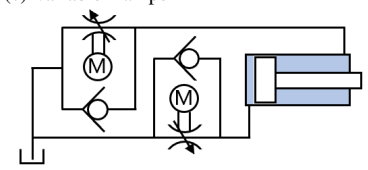
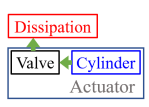
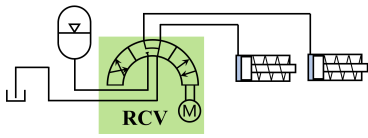
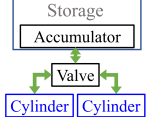
(b) Magnetorheological Clutch

A clutch based on the magnetorheological principle isolates the output from the motor, which increases safety. Hydrostatic transmission can be connected to an elastic container to give the output end a lower stiffness, providing higher compliance and better safety.

(c) Variable Damper

This scheme has no power source, provides passive force through variable damping, and cannot produce active joint torque to harm the wearer. The safety of this scheme has been demonstrated in many products of hydraulic prosthetic joints [9].

Table R1: Comparison of Hydraulic Actuation Schemes For Exoskeletons

Diagram	Energy Flow	Active or Passive	Study (year)	Features
<p>(a) Pump Driven System</p> 		Active	[2] (2022) [3] (2017) [4] (2017)	The most conventional scheme; Highly controllable; High energy consumption; Heavy system weight.
<p>(b) Magnetorheological Clutch</p>  <p>C: Coil B: Ball Screw</p>		Active	[5](2021) [6](2020)	Variable stiffness and damper; High compliance and safety; Low energy efficiency.
<p>(c) Variable Damper</p> 		Quasi-Passive	[7](2022) [8](2018) [9](2013)	Do only negative work; Long battery life; Compact and lightweight.
<p>(d) RCV Based Energy Regulation (this work)</p> 		Quasi-Passive	[10](2021) [11](2023)	High energy efficiency; Low energy consumption; Energy is harvested, stored, and released at different joint and time; Self-holding valve state.

(d) RCV Based Energy Regulation (this work)

1
2
3
4
5
6
7
8
9
10
11
12
13
14

1. This scheme has no power source for joint actuation, and all the pressure and power are generated from the energy harvested from walking motion. The output power thus could not exceed the power exerted by the wearer, which increases safety.

2. The steering motor of the RCV can be rotated by hand, and the angle of the valve core is self-holding. When the electric power runs out, the exoskeleton can be configured to the transparent mode manually, i.e., the cylinders are all inflated with low-pressure oil, without interfering with normal walking.

3. In order to improve the accuracy of gait recognition, we use both the rising edge of the forefoot sole pressure signal and the rapid change of toe flip angle as the signal of the toe-off event, thereby improving the fault tolerance rate and preventing stumble.

15
16
17
18
19

Due to the 11-page limit of the major revision, we have not included all of these points about safety in the manuscript, but have marked relevant expression about safety in Section I and V of the manuscript. If the manuscript meets the standards for acceptance, we will further summarize and discuss these points in the 12-page final version. Hope you can agree to our plan.

20
21
22
23
24
25

#2.2-4 The author has elucidated the novelty of the approach and drawn comparisons with other exoskeletons. Tables II and III demonstrate the efficacy of this method, suggesting that the proposed exoskeleton outperforms others in various aspects. Is this superiority only attributed to rotary cage valve? Could you kindly provide additional insights into the issues with other exoskeletons and how the proposed solution addresses these challenges?

26
27
28
29
30

Thanks for your recognition. The superiority of the proposed exoskeleton design is not solely attributed to the rotary cage valve but is a result of the combination of various innovative features and engineering advancements. Here lists the reasons why HyExo is superior to other exoskeletons. These points are also reflected in the manuscript.

31
32
33
34
35
36
37
38
39
40
41
42

1. The end support point of HyExo is set at the forefoot. There are some works investigating the important role of the torque generated by the Achilles tendon at the ankle joint in generating forward propulsion of the human body during the late stance phase [12, 13]. Most of the current load-bearing full-body exoskeletons transmit the load force to the ground at the support points on both sides of the ankle, but do not provide effective assistance to the ankle joint. This causes the heel lifting movement to be hindered by the downward support force transmitted by the exoskeleton during the late stance phase. There is a winch system at the ankle and toe joints, which is the key to saving ankle work. As shown in Fig. R2, the forefoot is in contact with the ground approximately 90% of the stance phase, while that of the heel is less than half. Therefore, setting the end of the exoskeleton near the toes helps the exoskeleton provide effective support for a longer period without affecting the lifting of the heel.



53
54
55
56
57
58
59
60

Figure R2: The key frames of a foot during its stance phase. The time interval between each frame of image is 0.03s. The red stripes mark the frames in which the heel is in contact with the ground, while the blue stripes mark the frames in which the forefoot is in contact with the ground.

1
2
3 **2.** The non-anthropomorphic design reduces unnecessary friction between the exoskeleton and the
4 human body and increases the force transmission efficiency. The kinematic pairs of most joints in the
5 human body are higher pairs, and the center of rotation is located inside the human body. Therefore,
6 the exoskeleton located outside the body with a small number of rotary joints has difficulty in com-
7 pletely following the movement of the human body segments. If the exoskeleton uses more degrees
8 of freedom to fit the human body segments, it will simultaneously increase the number of actuators in
9 series and reduce the load transfer efficiency. The misalignment of joints between the exoskeleton and
10 the human body will produce resistance during movement, which will lead to energy loss and a poor
11 wearing experience.

12 Non-anthropomorphic exoskeletons can reduce contact with the human body and focus on the transfer
13 of force between the load and the ground.

14 **3.** Hydraulic systems provide both high joint power density and high transparency. In most motor-
15 actuated legged system, there is a trade-off between higher output torque and higher speed. Motors
16 with higher gear ratio usually get lower speed and higher inertia, which slow down the response of the
17 system. That's why some motor-actuated exoskeleton has limited motion speed [14], but with high
18 loading capacity. On the contrast, Motors with lower gear ratio are insufficient in torque and energy
19 efficiency.

20 Hydraulic actuation can achieve both high torque and high transparency, the reason why RCV is
21 designed to have a large flow rate and fast response speed is because it can reduce the flow resistance,
22 and improve the response speed and energy efficiency of the system. Additionally, hydrostatic support
23 does not consume energy, which is consistent with the vertical support requirements of the exoskeleton
24 scenario.

25 **4.** Hydraulic oil, as a shapeless mechanical energy carrier, can be more flexibly modulated with
26 less constraints. Energy recovery works based on elastic elements are often limited to specific gait
27 patterns, and can only recycle energy between joints within a single gait cycle [15]. However, HyExo
28 can centralizedly manage the energy harvested and released by the joints at different times, which
29 increases the energy efficiency.

30
31
32
33
34 We thank Reviewer 2 for his/her constructive comments and suggestions.
35
36
37
38
39
40
41
42
43
44
45
46
47
48
49
50
51
52
53
54
55
56
57
58
59
60

Response to Reviewer # 3

#3.1 WHAT ARE THE CONTRIBUTIONS OF THIS PAPER: The study proposed a non-anthropomorphic lower-limb exoskeleton for gait assistance. The advantage of the design over other structures was less interference on human motions. The system was validated on human subjects, including walking tests and energy expenditure tests.

Thanks for the positive comments.

#3.2 WHAT ARE SOME WAYS IN WHICH THE PAPER COULD BE IMPROVED:

#3.2-1 The authors addressed most of the previous concerns from the reviewers. One thing is that the energy expenditure test was only conducted on one subject. The case report is less convincing than a systematic multi-subject experiment. Please add this point as one of limitations of current study.

Thanks for your suggestion. It may be that our expression in the paper was not clear enough, which caused you misunderstanding. A total of 8 subjects participated in the energy expenditure test to obtain statistically significant data. In Fig. 15, the markers with different shapes indicate every participant. We have improved the wording in the manuscript to reduce misunderstandings.

In the walking experiment described in Section IV.B, we only conducted the experiment on one subject. The walking experiment was designed to test the exoskeleton's load-carrying and energy modulation performance. In this experiment, we were more concerned with the differences of a individual subject under different experimental conditions than the differences between subjects or the overall results among subjects. Some previous studies also conducted experiments with one participant, and they successfully verified the effectiveness of their methods [6, 13]. Hope you can agree with our opinion.

#3.2-2 Another point is the attached video. The labels of the figures denoting the load carrying experiments can be optimized to give more information.

Thanks for your suggestion. Here we list the components of the video:

- 1. Performance of The Rotary Cage Valve(RCV) Block:** The RCV block shows a directional control demo, in which every RCV unit changes the valve position every 1 second.
- 2. Demonstration of DOFs:** The non-anthropomorphic structure allows for less interference with the wearer's body and basic locomotion. The people in the videos shows walk, step, turn, and abduction of the hip joint.
- 3. Load Sharing Effect:** The walking scene of the subject in the walking experiment in Section IV.B of the manuscript.
- 4. Impact on Gait at Different Speeds:** This part shows a subject's walking scene at speeds of 4km/h and 6km/h. For every speed, the three conditions were no HyExo, HyExo with the RCVs off, and HyExo with the RCVs on. This part corresponds to Section IV.C of the manuscript.

In the load sharing effect part of the video, we added the blue text of the set numbers on the supporting force graphs to mark the experimental conditions. Correspondingly, we marked the experimental details of each set in Section IV.B of the manuscript. We also modified the title of the HyExo's impact on gait part of the video.

We thank Reviewer 3 for his/her constructive comments and suggestions.

References

- [1] T. W. P. Huang and A. D. Kuo, "Mechanics and energetics of load carriage during human walking," *J. Exp. Biol.*, vol. 217, no. 4, pp. 605–613, 2014.
- [2] M. Sun, X. Ouyang, J. Mattila, Z. Chen, H. Yang, and H. Liu, "Lightweight electrohydrostatic actuator drive solution for exoskeleton robots," *IEEE/ASME Trans. Mechatronics*, vol. 27, no. 6, pp. 4631–4642, 2022.
- [3] H. Kim, Y. J. Shin, and J. Kim, "Design and locomotion control of a hydraulic lower extremity exoskeleton for mobility augmentation," *Mechatronics*, vol. 46, pp. 32–45, 2017.
- [4] J. Zhu, Y. Wang, J. Jiang, B. Sun, and H. Cao, "Unidirectional variable stiffness hydraulic actuator for load-carrying knee exoskeleton," *International Journal of Advanced Robotic Systems*, vol. 14, no. 1, p. 1729881416686955, 2017. [Online]. Available: <https://doi.org/10.1177/1729881416686955>
- [5] C. Véronneau, J. Denis, L.-P. Lebel, M. Denninger, V. Blanchard, A. Girard, and J.-S. Plante, "Multifunctional remotely actuated 3-dof supernumerary robotic arm based on magnetorheological clutches and hydrostatic transmission lines," *IEEE Robotics and Automation Letters*, vol. 5, no. 2, pp. 2546–2553, 2020.
- [6] C. Khazoom, P. Caillouette, A. Girard, and J.-S. Plante, "A supernumerary robotic leg powered by magnetorheological actuators to assist human locomotion," *IEEE Robot. Automat. Lett.*, vol. 5, no. 4, pp. 5143–5150, 2020.
- [7] M. Kennard, K. Yagi, M. Hassan, H. Kadone, H. Mochiyama, and K. Suzuki, "Variable-damper control using mr fluid for lower back support exoskeleton," *IEEE/ASME Transactions on Mechatronics*, vol. 28, no. 1, pp. 579–587, 2023.
- [8] W. van Dijk, T. Van de Wijdeven, M. Holscher, R. Barents, R. Könemann, F. Krause, and C. Koerhuis, "Exobuddy - a non-anthropomorphic quasi-passive exoskeleton for load carrying assistance," in *Proc. IEEE Int. Conf. Biomed. Robot. Biomechat.*, Twente, Netherlands, 2018, pp. 336–341.
- [9] J. Thiele, B. Westebbe, M. Bellmann, and M. Kraft, "Designs and performance of microprocessor-controlled knee joints," *Biomedizinische Technik/Biomedical Engineering*, vol. 59, no. 1, pp. 65–77, 2014. [Online]. Available: <https://doi.org/10.1515/bmt-2013-0069>
- [10] W. Fan, T. Liu, J. Yi, X. Huang, B. Zhang, X. Zhang, and S. Wang, "A passive hydraulic auxiliary system designed for increasing legged robot payload and efficiency," in *Proc. IEEE Int. Conf. Robot. Autom.*, Xi'an, China, 2021, pp. 3097–3103.
- [11] Wu, Fan and Zhe, Dai and Wenyu, Li and Xiufeng, Zhang and João, Paulo Ferreira and Tao, Liu , "A rotary-cage valve (rcv) for variable damper in prosthetic knee," https://www.researchgate.net/publication/374004111_A_Rotary-Cage_Valve_RCV_for_Variable_Damper_in_Prosthetic_Knee, 2023, [Online; accessed 19-September-2023].
- [12] S. H. Collins, M. B. Wiggin, and G. S. Sawicki, "Reducing the energy cost of human walking using an unpowered exoskeleton," *Nature*, vol. 522, no. 7555, pp. 212–215, 2015.
- [13] J. Chen, J. Han, and J. Zhang, "Design and evaluation of a mobile ankle exoskeleton with switchable actuation configurations," *IEEE/ASME Transactions on Mechatronics*, vol. 27, no. 4, pp. 1846–1853, 2022.

1
2
3
4
5
6
7
8
9
10
11
12
13
14
15
16
17
18
19
20
21
22
23
24
25
26
27
28
29
30
31
32
33
34
35
36
37
38
39
40
41
42
43
44
45
46
47
48
49
50
51
52
53
54
55
56
57
58
59
60

[14] (2020) Guardian xo full-body powered exoskeleton. [Online]. Available: <https://www.sarcos.com/products/guardian-xo-powered-exoskeleton/>

[15] H. Shi, Z. Liu, and X. Mei, "Overview of human walking induced energy harvesting technologies and its possibility for walking robotics," *Energies*, vol. 13, no. 1, p. 86, 2019.

Supplementary Materials for HyExo: A Novel Quasi-Passive Hydraulic Exoskeleton for Load-Carrying Augmentation

Wu Fan, Zhe Dai, Bin Zhang, Long He, Min Pan, and Jingang Yi, Tao Liu

A. Frequency Response of RCV

The frequency response of RCV was tested by the position tracking experiment, in which the target angle of the inner cage is a sinusoidal curve with increasing frequency. The experimental results are shown in Fig. S1.

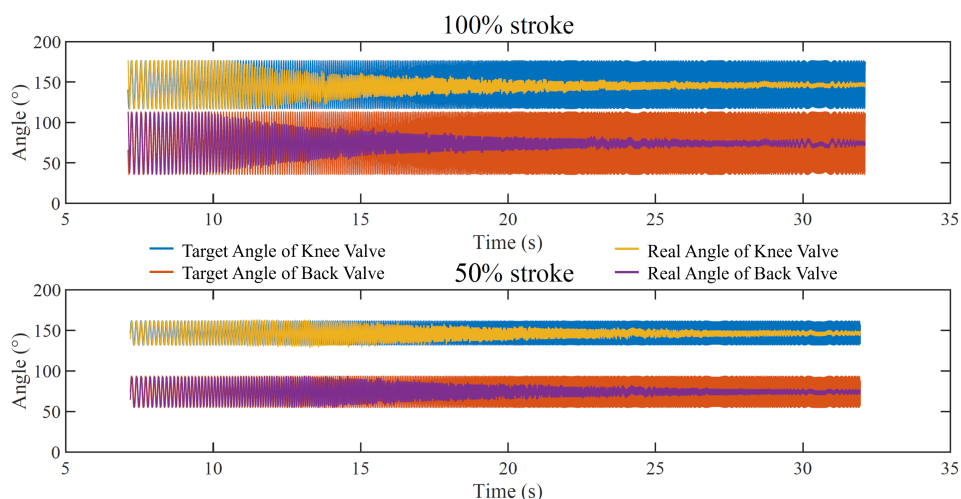


Fig. S1: The position tracking results of RCV in time domain.

The resultant bode plot is shown in Fig. S2.

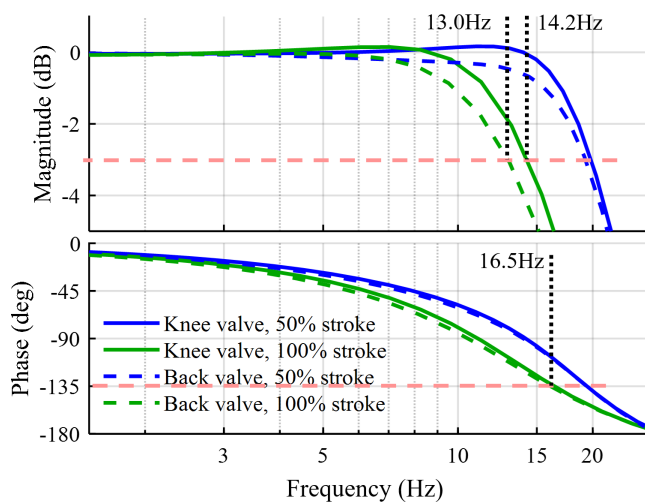


Fig. S2: The frequency response of the RCV in position tracking test.

W. Fan, T. Liu, and Z. Dai are with the State Key Laboratory of Fluid Power & Mechatronic Systems, School of Mechanical Engineering, Zhejiang University, 310027, Hangzhou, China (e-mail: zjufanwu@zju.edu.cn; dai zhe@zju.edu.cn; liutao@zju.edu.cn).

B. Zhang is with the College of Mechanical and Electrical Engineering, China Jiliang University, Hangzhou 310018, zhangbin@cjlu.edu.cn

L. He is with the Zhiyuan Research Institute, 310024, Hangzhou, China (e-mail: helong@zy-cs.com.cn).

M. Pan is with the Department of Mechanical Engineering at the University of Bath, BA2 7AY Bath, UK (e-mail: mp351@bath.ac.uk).

J. Yi is with the Department of Mechanical and Aerospace Engineering, Rutgers University, Piscataway, NJ 08854 USA (e-mail: jgyi@rutgers.edu).

B. Step Response of RCV

The energy consumption and switching time were measured in the step response experiment. As shown in Fig. S3, the current and angle of the inner cage of a 40° switching action of the back valve and a 60° switching action of the knee valve are plotted. The rise time (i.e., the time taken for the response from 10% to 90% of the way from the initial value to steady-state value) is marked as green annotation.

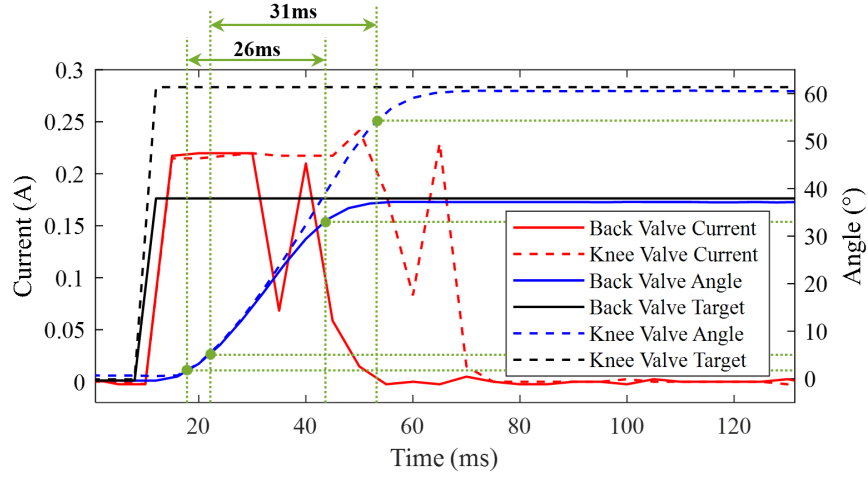


Fig. S3: The step response of the knee valve and the back valve.

C. The Dynamics of Free Bodies

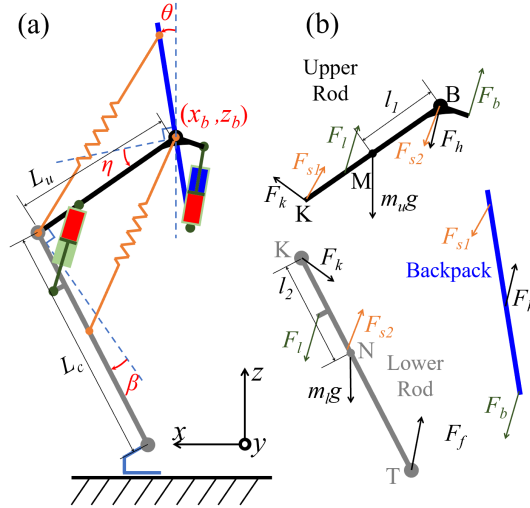


Fig. S4: The force analysis diagrams of HyExo in the sagittal plane. (a) is the definition of HyExo's degrees of freedom. (b) is the free body diagram of the three parts of the exoskeleton.

For the upper leg, its angular acceleration α_u and acceleration \mathbf{a}_{uc} can be expressed as below,

$$\begin{cases} \alpha_u = \ddot{\eta} + \ddot{\theta}, \quad \omega_u = |\dot{\eta} + \dot{\theta}|, \\ \mathbf{a}_{uc} = \begin{bmatrix} \ddot{x}_b \\ \ddot{z}_b \end{bmatrix} + \omega_u^2 \overrightarrow{MB} + \alpha_u \times \overrightarrow{BM}, \end{cases} \quad (S1)$$

where ω_u is the angular velocity of the upper rod. \overrightarrow{MB} and \overrightarrow{BM} are the space vectors between point B and M, as shown in Fig. S4(b). For the lower leg, its angular acceleration α_l and acceleration \mathbf{a}_{lc} can be expressed as below,

$$\begin{cases} \alpha_l = \ddot{\eta} + \ddot{\theta} - \ddot{\beta}, \quad \omega_l = |\dot{\eta} + \dot{\theta} - \dot{\beta}|, \\ \mathbf{a}_{lc} = \begin{bmatrix} \ddot{x}_b \\ \ddot{z}_b \end{bmatrix} + \omega_u^2 \overrightarrow{KB} + \alpha_u \times \overrightarrow{BK} + \omega_l^2 \overrightarrow{NK} + \alpha_l \times \overrightarrow{KN}, \end{cases} \quad (S2)$$

where ω_l is the angular velocity of the lower rod. \overrightarrow{KB} , \overrightarrow{BK} , \overrightarrow{NK} , and \overrightarrow{KN} are the space vectors depicted in Fig. S4(b).

D. Comparison of State-of-The-Art Exoskeletons

TABLE S1: State-of-the-Art Weight-Bearing Exoskeleton (or Supernumerary Leg) Comparison



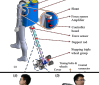

















Study (year)	Picture	Rated Speed (km/h)	Mean Support Force (N)	Power (W)	Q (kmN/W/h)	Active or Passive	Self Weight	Major Effect
Khazoom <i>et al.</i> [1] (2020)		5	293	84	17.4	Active	9.7 (one leg)	A theoretical upper limit suggests that the average transmitted power in a gait cycle could be 84 W for the leader-follower gait, which is 4 times higher than autonomous ankle exoskeletons.
Leng <i>et al.</i> [2] (2021)		5	80	24.65	16.2	Active	1.77	The WRL_ON condition has reduced the vertical load force on the human, the vertical ground reaction force of human feet, and the metabolic power by 32.29%, 8.08% and 18.92% during walking.
Yang <i>et al.</i> [3] (2022)		1.08	490.78 – 417.46 = 73.3	-	-	Active	14.5	Centaur system can effectively reduce 70.03% of the peak force with load carriage.
Xiang <i>et al.</i> [4] (2021)		2.88	110	-	-	Active	10.8	The system could lower metabolic power consumption by 12.56% and 5.42% during standing, and 36.58% and 20.85% during walking.
Hao <i>et al.</i> [5] (2020)		2.5	66.3	4.07	40.7	Active	8.7	SuperLimb system can reduce 85.7% of load weight borne by the human when both robotic limbs support and 55.8% load weight on average.
Zhou <i>et al.</i> [6] (2021)		3.5	$15.8 \times 9.8 \times$ $24.6\% = 38.1$	0	-	Passive	4.5	The exoskeleton can transfer on average 68.0% of the load (15.8kg) to the ground while standing, and 24.6% of the load while walking. The maximum load is reduced by 22.1% during walking.
Wang <i>et al.</i> [7] (2020)		2	441	-	-	Active	27.8	PALExo has load-bearing effect when walking with loads, but there are certain problems in the excessive process when the legs switching between the swing phase and the stance phase.
HERCULE [8] (2010)		4	1000	-	-	Active	24.8	It can carry a load of 100kg and its battery enables the wearer to walk 20km at a moving speed of 4km/h.
Zoss <i>et al.</i> [9] (2005)		4.7	735	2270	1.5	Active	34	BLEEX has been demonstrated to support up to 75 kg (exoskeleton weight + payload), walk at speeds up to 1.3 m/s, and shadow the operator through numerous maneuvers without any human sensing or pre-programmed motions.
Dijk <i>et al.</i> [10] (2018)		5.7	130	-	-	Quasi-Passive	21.8	The quasi-passive mechanism led only to a small, non-significant, increase in energy expenditure. Exobuddy unloaded the subjects by transferring on average approximately 30% (130 N) of the load to the ground with a maximum of 53% right after heel strike.
Gregorczyk <i>et al.</i> [11] (2010)		4.824	$(75.1 + 55) \times$ $(12.7 - 11.3) =$ 182.1	-	-	Quasi-passive	15	EXO increased users' metabolic cost while carrying various loads and altered their gait biomechanics compared with conventional load carriage.
Ikeuchi <i>et al.</i> [12] (2009)		5.7	130	-	-	Quasi-Passive	21.8	The quasi-passive mechanism led only to a small, non-significant, increase in energy expenditure. Exobuddy unloaded the subjects by transferring on average approximately 30% (130 N) of the load to the ground with a maximum of 53% right after heel strike.
Walsh <i>et al.</i> [13] (2007)		3.3	$36 \times 9.8 \times$ $0.8 \times (0.55 -$ $0.15) / 1 \times 2 =$ 225.8	2	372.57	Quasi-Passive	11.7	The exoskeleton slightly increases the walking metabolic cost of transport (COT) as compared to a standard loaded backpack (10% increase).
This work (2023)		4	237	1.6	592.5	Quasi-Passive	13.87	The exoskeleton slightly increases the walking metabolic cost of transport (COT) as compared to a standard loaded backpack (10% increase).

TABLE S2: Weight-Bearing Exoskeleton in the Market

Study (year)	Picture	Speed (km/h)	Support Force (N)	Power (W)	Q (kmN/W/h)	Active or Passive	Self Weight	Product Features & Our Perspective
Sarcos Robotics, Guardian XO [14] (2020)		-	889	-	-	Active	113	The full-body exoskeleton represented by Guardian XO has a heavy weight, but can dynamically compensate for gravity and inertia. Due to the greater energy consumption, heavier weights can be lifted. The large torque of the joint motors also leads to a high inertia and limited walking speed.
ULS Robotics, BES-PRO [15] (2023)		4.8	-	-	-	Active	18	BES-PRO is designed to enable universities, R&D institutions and medical research centers to conduct further development and research. It can be used for 3-4 hours on a single charge. For such motor-driven exoskeletons, there is a trade-off between maximum joint torque and maximum angular velocity.
NIUDI TECH, PULEE [16] (2020)		7	$25 \times 30\% \times 9.8 = 73.5$	0	-	Passive	6	PULEE is a completely passive exoskeleton designed to transmit partial load to the ground. It is lightweight and flexible, allowing for actions such as running, jumping, squatting, and even crawling. It achieves 50% load transfer during static standing, but the load transfer effectiveness may be reduced during walking.
SEEPPO TECH, Aload-H [17] (2023)		-	$35 \times 45\% \times 9.8 = 154.4$	0	-	Passive	5.5	SEEPPO Aload-H can reduce the force exerted on the human body by 45% while walking and 70% while standing. Due to its portability and flexibility, it is expected to be applied in firefighting and emergency rescue or outdoor work with heavy lifting requirements.
Lockheed Martin, Fortis [18] (2017)		-	222	0	-	Passive	-	Fortis is an aluminum and carbon fiber framed exoskeleton with mechanical arms designed to give tools a zero-gravity weightless feel. It lets workers in variety of industries wield heavy tools for hours on end. It is designed for long periods of static postures, and the walking assistance effect is unknown.
Noonee, Chairless Chair 2.0 [19] (2020)		-	1176	0	-	Passive	2.95	The Chairless Chair 2.0 is a wearable ergonomic mechanical device intended for use in production and assembly lines. It allows users to take breaks and be able to sit down from time to time while working. It does not interfere with walking, but it also cannot provide assistance while walking.
PCONhac, N-2 Bionics [20] (2020)		-	-	0	-	Passive	-	N-2 Bionics has innovatively placed the weight platform and exoskeleton on the front side of the human body, which brings the load center closer to the ground contact point. However, this design may not accommodate larger strides, and the variable upper leg length design during gait can cause impacts at higher walking speeds.

E. Feasibility of toe flip angle signal as a trigger

To validate the Feasibility of toe flip angle signal as a trigger, we supplemented several tests on different terrains, including stair ascent and stair descent. As shown in Fig. S5, the green boxes indicate that whether walking on level ground, ramps, or stairs, using toe extension angle as a trigger of phase change is feasible because there is always a sharp rise of the toe flip angle when the toe-off occurs. Besides the toe extension signal, the rising edge of the forefoot pressure signal is also set as the trigger of phase change to avoid stumbling, so that the safety of foot lifting is guaranteed.

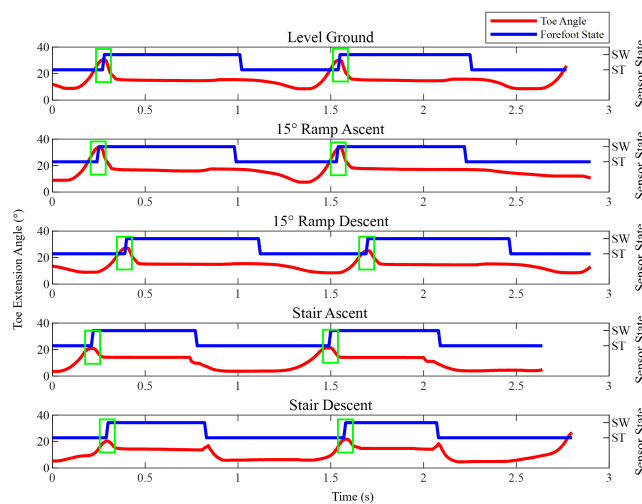


Fig. S5: Toe extension angle and forefoot phase on level ground, ramp ascent, ramp descent, stair ascent, and stair descent.

REFERENCES

- [1] C. Khazoom, P. Caillouette, A. Girard, and J.-S. Plante, "A supernumerary robotic leg powered by magnetorheological actuators to assist human locomotion," *IEEE Robot. Automat. Lett.*, vol. 5, no. 4, pp. 5143–5150, 2020.
- [2] Y. Leng, X. Lin, G. Huang, M. Hao, J. Wu, Y. Xiang, K. Zhang, and C. Fu, "Wheel-legged robotic limb to assist human with load carriage: An application for environmental disinfection during COVID-19," *IEEE Robot. Automat. Lett.*, vol. 6, no. 2, pp. 3695–3702, 2021.
- [3] P. Yang, H. Yan, B. Yang, J. Li, K. Li, Y. Leng, and C. Fu, "A centaur system for assisting human walking with load carriage," in *2022 IEEE/RSJ International Conference on Intelligent Robots and Systems (IROS)*, 2022, pp. 5242–5248.
- [4] Y. Xiang, X. Yan, H. Su, N. Chen, S. Guo, J. Wu, Y. Leng, and C. Fu, "Powered super tail: A terrain-adaptive wheel-legged robotic limb to assist human's load carriage," in *2021 27th International Conference on Mechatronics and Machine Vision in Practice (M2VIP)*, 2021, pp. 676–681.
- [5] M. Hao, J. Zhang, K. Chen, H. Asada, and C. Fu, "Supernumerary Robotic Limbs to Assist Human Walking With Load Carriage," *Journal of Mechanisms and Robotics*, vol. 12, no. 6, p. 061014, 07 2020. [Online]. Available: <https://doi.org/10.1115/1.4047729>
- [6] Z. Zhou, W. Chen, H. Fu, X. Fang, and C. Xiong, "Design and experimental evaluation of a non-anthropomorphic passive load-carrying exoskeleton," in *2021 6th IEEE International Conference on Advanced Robotics and Mechatronics (ICARM)*, 2021, pp. 251–256.
- [7] T. Wang, Y. Zhu, T. Zheng, D. Sui, S. Zhao, and J. Zhao, "Palexo: A parallel actuated lower limb exoskeleton for high-load carrying," *IEEE Access*, vol. 8, pp. 67 250–67 262, 2020.
- [8] Exoskeleton Report, "Hercule," <https://exoskeletonreport.com/product/hercule/>, 2016, [Online; accessed 23-September-2023].
- [9] A. Zoss, H. Kazerooni, and A. Chu, "On the mechanical design of the Berkeley lower extremity exoskeleton (BLEEX)," in *Proc. IEEE/RSJ Int. Conf. Intell. Robot. Syst.*, Edmonton, Canada, 2005, pp. 3465–3472.
- [10] W. van Dijk, T. Van de Wijdeven, M. Holscher, R. Barents, R. Könemann, F. Krause, and C. Koerhuis, "Exobuddy - a non-anthropomorphic quasi-passive exoskeleton for load carrying assistance," in *Proc. IEEE Int. Conf. Biomed. Robot. Biomechat.*, Twente, Netherlands, 2018, pp. 336–341.
- [11] J. M. S. C. K. B. J. P. O. Karen N. Gregorczyk, Leif Hasselquist and D. J. Gutekunst, "Effects of a lower-body exoskeleton device on metabolic cost and gait biomechanics during load carriage," *Ergonomics*, vol. 53, no. 10, pp. 1263–1275, 2010. [Online]. Available: <https://doi.org/10.1080/00140139.2010.512982>
- [12] Y. Ikeuchi, J. Ashihara, Y. Hiki, H. Kudoh, and T. Noda, "Walking assist device with bodyweight support system," in *2009 IEEE/RSJ International Conference on Intelligent Robots and Systems*, 2009, pp. 4073–4079.
- [13] C. J. Walsh, K. Endo, and H. Herr, "A quasi-passive leg exoskeleton for load-carrying augmentation," *Int. J. Humanoid Robot.*, vol. 4, no. 3, pp. 487–506, 2007.
- [14] (2020) Guardian xo full-body powered exoskeleton. [Online]. Available: <https://www.sarcos.com/products/guardian-xo-powered-exoskeleton/>
- [15] (2023) Uls robotics bes-pro lower limb exoskeleton. [Online]. Available: <https://www.ulsrobotics.com/h-col-117.html>
- [16] (2020) Pulee (passive augmenting lower extremity exoskeleton). [Online]. Available: <https://www.niudi.tech/product1.html>
- [17] (2023) Load-bearing mobile exoskeleton aload-h. [Online]. Available: <https://www.shipengexo.com/productinfo1.html#>
- [18] (2020) Let the fortis® tool arm give you a hand! [Online]. Available: <https://www.niudi.tech/product1.html>
- [19] (2020) Chairless chair 2.0 – the new generation. [Online]. Available: <https://www.noonee.com/the-chairless-chair-2-0/?lang=en>
- [20] (2020) N-2 bionics - the world's first wearable baby weight supporting device. [Online]. Available: <https://twitter.com/NhacPco>

LIST OF FIGURES

1			
2			
3	1	(a) HyExo's non-anthropomorphic architecture and DOFs. The blue arrows represent the axis of motion joints, and the violet curved arrows indicate three rotary DoFs at TP. The green transparent plane indicates that the TP, KP, and BP are in a plane perpendicular to the knee joint axis (Z_3). (b) The main components and several close-up shots of key parts. (c) A list of component weights.	2
4			
5			
6			
7	2	(a) The hydraulic circuit of HyExo. Red lines represent high pressure, and blue lines represent low pressure. (b) The front and back view of RCV block. (c) The section view of half an RCV block. The red and blue chambers are inflated with high- and low-pressure oil, respectively. Port A and C connect to the rodless side of the back and knee cylinders, respectively, and Port B connects to the rod side of the back cylinder. (d) The four-bar steering linkage of the RCV's actuator. (e) Each pair of rotary cages consists of an inner cage (spool) and an outer cage (sleeve).	3
8			
9			
10			
11			
12			
13	3	The force analysis diagrams of HyExo in the sagittal plane. (a) is the definition of HyExo's degrees of freedom. (b) is the free body diagram of the three parts of the exoskeleton. (c) is the interaction diagram between the wearer and HyExo.	4
14			
15			
16	4	The visualization of the man-machine interaction force of an entire gait cycle in simulation. Black lines are the keyframes of one leg's rods. Green arrows represent the force vectors F_f at TP during the swing phase, and cyan arrows represent the resultant force F_r , which is the sum of F_{s1} , F_h , and F_b on the backpack during the stance phase. The purple and magenta arrows represent the F_r when only the back cylinder is activated and only the knee cylinder is activated, respectively.	4
17			
18			
19			
20			
21	5	The schematic diagram of the HyExo control design. (a) The coordination of the HyExo control with wearer walking gait. (b) The corresponding state (open and close) of the knee and back cylinders. B_i and K_i , $i = 1, 2$, are the state codes of different connection of cylinders. (c) The HyExo control block diagram.	5
22			
23			
24	6	In a gait cycle, the flip angle of toe joint ϵ shows a sharp increase at the end of stance phase. The heel sensor and forefoot sensor are the force sensor based on FSR shown in Fig. 1(b).	5
25			
26	7	The illustrative diagram of cylinder length of a knee cylinder and the ipsilateral back cylinder. The lengths of extension of the back cylinder (red line) and contraction of the knee cylinder (black line) are the same during the stance phase.	5
27			
28			
29	8	The schematic of energy regulation to determine switching time t_s	6
30	9	The switching timing t_s^* optimized by Algorithm 1 when ΔV is not zero.	6
31	10	The 6-DOFs of HyExo is demonstrated in motions such as stepping, abduction of the hip, and waist twisting.	7
32	11	The forces measured by the load cell at TP in sets 3,2 and 1. The blue, red and gray stripes are the gait phase of legs.	7
33			
34	12	(a) The length variations of the back cylinder and the knee cylinder during the stance phase. The dash lines are the hyperplane between two adjacent data sets. (b) The calculated mean force transformed to the ground by an unilateral leg during the whole gait cycle.	7
35			
36			
37	13	Photos of a participant walking in the control group (first row) and in the HyExo-on group (second row).	8
38	14	The joint angle of hip, knee, and ankle averaged across participants, with the error bars of key extremum points.	8
39	15	The metabolic cost (mean and standard deviation) of 8 subjects at six different testing stages. The markers with different shapes indicate every participant. The dashed lines indicate the increasing trend of metabolic rate with the increase of load. k_1 and k_2 are the slope of the linear regression result.	9
40			
41			
42			

LIST OF TABLES

44	I	The statistic result of the p -value in paired t-test between different groups.	8
45	II	Comparison with representative products	10
46	III	Comparison of Load-Supporting Exoskeletons	10
47			
48			
49			
50			
51			
52			
53			
54			
55			
56			
57			
58			
59			
60			